Chapter XI

LOCALIZATION PHENOMENA AND REGULARIZATION METHODS

by S. Forest and E. Lorentz

1 STRAIN LOCALIZATION CRITERIA IN ELASTOVISCOPLASTIC SOLIDS

The modeling of damage processes at the material point scale through a specific constitutive law addresses a wide variety of constitutive behaviors, for instance brittle elasticity where the evolution of damage degrades the elastic stiffness, or ductile plasticity where both dissipative mechanisms (plasticity and damage) are intimately coupled. In spite of their obvious differences, all these laws possess a common feature: beyond some load level, the domain of reversibility expressed in the stress space shrinks. This phenomenon is called strain-softening. This essential property, characteristic of damage mechanisms, is responsible for the localization of the mechanical fields (strain, damage, plastic strain, ...) inside narrow bands, an experimental fact observed on many degrading materials such as soils, concrete, metals, etc., see for instance Desrues and Chambon (1985).

Despite twenty years of intensive research, numerical modeling of the localization phenomenon remains a challenging objective which has not yet been given a fully satisfactory answer. This is in contrast with the great progresses that have been achieved regarding the local description of damage mechanisms for various materials, on the basis of micro–macro derivations as well as phenomenological intuitions. Unfortunately, localization partially hinders predictive computations of propagating damaged zones in real-life structures submitted to a given load history.

The difficulty originates from the fact that the equations that describe the structural behavior (including not only the constitutive law but also the equilibrium and compatibility equations) result in an ill-posed problem which manifests itself by a spurious mesh-dependency when making use of finite element solutions.

After a first insight into the localization phenomena, the problem of loss of uniqueness and loss of ellipticity is addressed for elastoplastic solids. General (diffuse) and localized bifurcation modes are distinguished. The existence of jumps of the velocity gradient is explored in the dynamic (acceleration waves) and static cases (stationary waves). Critical values of hardening moduli for loss of uniqueness or loss of ellipticity are derived. A link between the notion of material stability and acceleration waves is also presented. The collected strain localization criteria are summarized in section 1.2.6.

Note that the derivations and formula are presented in the case of elastoplastic materials. However the results can be extended to damaging materials in a straightforward

manner. In fact it deals with all incremental models involving a fourth–rank tangent operator $\underset{\approx}{\mathbf{L}}$.

1.1 THE LOCALIZATION PHENOMENON: A FIRST INSIGHT

1.1.1 One–dimensional example

The afore-mentioned spurious mesh-dependency is easily observed through the analysis of a rod of length L which obeys a brittle elastic law, see figure XI.1. Due to the 1D character of the structure, the strain and stress fields are scalar, respectively ε and σ. Moreover, the equilibrium equation states that the stress is homogeneous:

$$\frac{\partial \sigma}{\partial x} = 0 \tag{1}$$

The rod is clamped at one end and submitted to an increasing displacement U at the other end: as we restrict our attention to a rate-independent behavior, the physical time does not play any role so that U is the only loading parameter. Thanks again to the 1D character, the compatibility equation on the strain field simply reads:

$$\int_0^L \varepsilon \, dx = U \tag{2}$$

Finally, the constitutive law has to be stated. While the strain remains smaller than a critical value ε^y, the stress – strain relation is linear elastic with stiffness E:

$$\sigma = E\,\varepsilon \quad \text{if } \varepsilon \leq \varepsilon^y \tag{3}$$

Above the critical value, the stress is a decreasing affine function of the strain, with slope $-H$, up to a vanishing stress that corresponds to the complete fracture of the rod:

$$\sigma = E\,\varepsilon^y \; - H \; (\varepsilon - \varepsilon^y) \quad \text{if } \varepsilon > \varepsilon^y \tag{4}$$

The law should also include a description of elastic unloading branches but, as a monotonous load history is only considered, they are ignored in the present example. Such a law indeed exhibits strain-softening since the threshold stress (4) decreases with the load history.

At this stage, the set of equations (1) to (4) totally describes the problem. A solution can be built by distinguishing two successive regimes.

First, while the load parameter is small enough, the behavior remains elastic, thus obeying (3), and therefore, thanks to the equilibrium equation (1), the strain field is homogeneous too. The compatibility equation (2) finally provides the strain value and the constitutive law (3) the stress value:

$$\forall\, x \quad \varepsilon(x) = \frac{U}{L} \quad \sigma(x) = \frac{E\,U}{L} \tag{5}$$

As an elastic behavior has been assumed, the strain should remain lower than ε^y, so that this regime is licit while $U \leq L\,\varepsilon^y$.

When this critical load is reached, the (homogeneous) stress cannot increase anymore. At each material point, there are two possible branches for its decrease. A damaging unloading obeying law (4) which takes place in a region Ω_D of length l

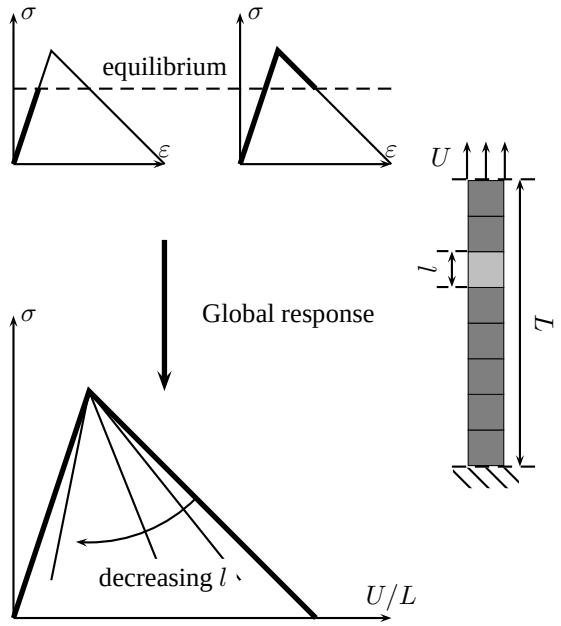

Figure XI.1: Localization in a 1D rod specimen

and an elastic unloading (3) in a region Ω_E of length $L - l$. As the stress field is still homogeneous, thanks to the equilibrium equation (1), the strain values in the damaging area and in the elastic area are respectively given by:

$$\begin{cases} \forall\, x \in \Omega_D & \varepsilon(x) = \varepsilon^y + \dfrac{E\,\varepsilon^y - \sigma}{H} \\ \forall\, x \in \Omega_E & \varepsilon(x) = \dfrac{\sigma}{E} \end{cases} \tag{6}$$

The compatibility equation then allows the determination of the stress:

$$l\left(\varepsilon^y + \frac{E\varepsilon^y - \sigma}{H}\right) + (L-l)\,\frac{\sigma}{E} = U \quad \Rightarrow \quad \frac{\sigma}{E\varepsilon^y} = \frac{\dfrac{U}{L\varepsilon^y} - \dfrac{l}{L}\left(1 + \dfrac{E}{H}\right)}{1 - \dfrac{l}{L}\left(1 + \dfrac{E}{H}\right)} \tag{7}$$

The global response of the rod is plotted on figure XI.1 in terms of the homogeneous stress versus the applied displacement. It appears that the response depends on the length of the damaged zone and may even exhibit a snap-back. Actually, the essential point is that the length of the damaged zone remains undetermined: there exists an infinity of linearly independent solutions, hence the problem is ill-posed.

When considering the solution of the problem using finite elements, say linear finite elements, the strain field is approximated by piecewise constant functions, that is the length of the damaged zone is necessarily a multiple of the size of a single element. Because of round-off errors or stress concentrations due to geometrical imperfections (cross-section of the rod), one finite element reaches the threshold slightly before the

others: the damaged zone then coincides with a single finite element. Therefore, it means that damage localizes in a narrow band of width the size of one finite element. The global response depends spuriously on the size of the finite elements and tends to a pure elastic unloading when the size goes to zero: at the limit, the computation would even predict that the rod breaks without dissipating energy, an aberrant result.

1.1.2 Consequences on the modeling of real-life structures

In the previous example, a spurious mesh dependency has been exhibited for a 1D structure made of an academic strain-softening material: the damage and the strain fields tend to localize in a single finite element, although the constitutive law is well defined. The bifurcation from the homogeneous solution to the localized one is in agreement with experimental observations. But the extreme dependence of the solution on the size of the finite elements dramatically raises the question of the ability to predict the response of a damaging structure through finite element computations. This is even more critical in the context of 2D or 3D simulations since the numerical solution depends not only on the size but also on the orientation of the finite elements (actually, it depends on all the mesh characteristics).

To illustrate the question of mesh-dependency related to the inception and the propagation of damaged zones in 2D structures, the perforated plate depicted in figure XI.2 is considered. The upper and lower sides are subjected to a prescribed vertical displacement (opposite on both sides, thus symmetric). The numerical simulations are performed under the assumption of plane strain. Traction stresses are expected to concentrate in the vicinity of the hole on th right and left handside, so that damage will be triggered in this area before propagating in mode I toward the closest free side of the specimen (right) then toward the other one (left), up to final fracture of the specimen. The constitutive law is one of the simplest that includes strain-softening. It appears as a 3D extension of the law used in the previous section since its response still corresponds to a linear softening when submitted to a proportional load. In addition to the usual elastic characteristics (isotropic Hooke's tensor $\underset{\approx}{\mathbf{E}}$, with Young modulus E and Poisson ratio ν), two parameters describe the local response of a material point: the maximal stress σ^y that the material can sustain (or equivalently the peak strain ε^y) and the (volume) energy dissipated when a material point is fully fractured (or equivalently the normalized softening slope γ), see figure XI.3.

More precisely, the material state is characterized by the strain tensor $\underset{\sim}{\varepsilon}$ and a scalar damage internal variable d ranging from 0 (sound material) to 1 (totally damaged material, $i.e.$ with zero residual stiffness). The stress – strain relation is elastic ; the stiffness is a linear decreasing function of the damage:

$$\underset{\sim}{\sigma} = (1-d)\,\underset{\approx}{\mathbf{E}} : \underset{\sim}{\varepsilon} \tag{8}$$

The increasing damage evolution is governed by the following threshold function and the corresponding consistency condition, expressed in terms of the volumetric dissipated energy k and the normalized softening slope γ:

$$g\left(\underset{\sim}{\varepsilon},\, d\right) = \frac{1}{2}\,\underset{\sim}{\varepsilon} : \underset{\approx}{\mathbf{E}} : \underset{\sim}{\varepsilon} - w^y\,(d) \qquad \text{where} \quad w^y\,(d) = \frac{k\,\gamma\,(1+\gamma)}{(1+\gamma-d)^2} \tag{9}$$

$$g\left(\underset{\sim}{\varepsilon},\, d\right) \leq 0 \qquad \dot{d} \geq 0 \qquad \dot{d}\; g\left(\underset{\sim}{\varepsilon},\, d\right) = 0 \tag{10}$$

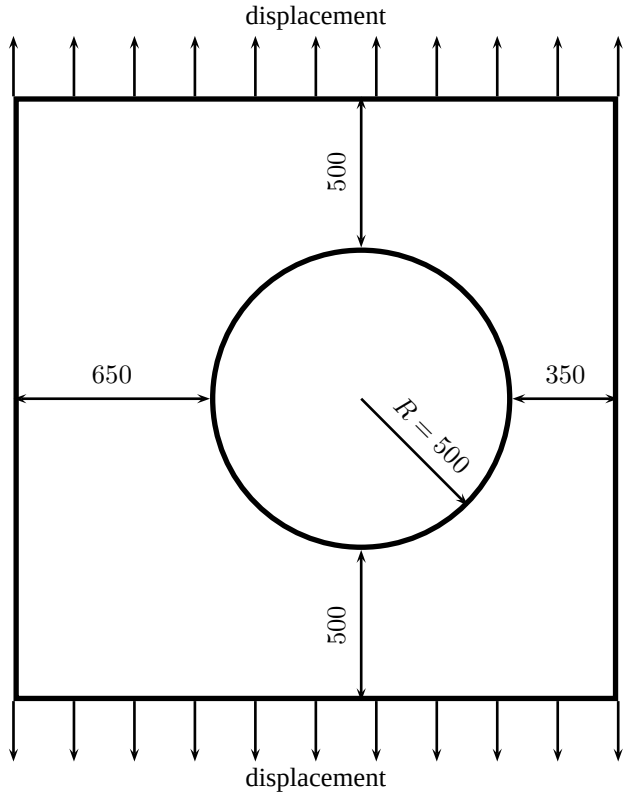

Figure XI.2: Perforated plate: geometry (in mm) and loading conditions

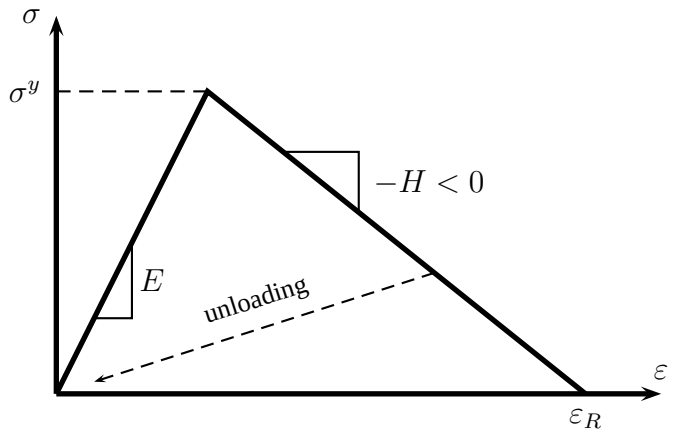

Figure XI.3: Brittle damage law: response of a material point under uniaxial tension

In spite of its simplicity (namely, there is no distinction between compressive and tensile states and brittle damage is the only dissipative mechanism), the law includes strain-softening (shrinkage of the elastic domain in the stress-space), the essential feature that will induce spurious damage localization:

$$g\left(\underset{\sim}{\varepsilon},\, d\right) \leq 0 \qquad \Rightarrow \qquad \frac{1}{2}\,\underset{\sim}{\sigma} : \underset{\approx}{\mathbf{E}}^{-1} : \underset{\sim}{\sigma} \quad \leq \quad \underbrace{\frac{k\,\gamma\,(1+\gamma)\,(1-d)^2}{(1+\gamma-d)^2}}_{\text{decreasing function of } d} \tag{11}$$

The material parameters are given in table XI.1. Numerical simulations have been conducted with two different meshes, see figure XI.4: the first one is an unstructured mesh based on linear triangles, the second one includes an oriented band of quadrangles dived into unstructured triangles. It can be noticed that the second one is more refined than the first one. We just mention that because of the instabilities that have already been exhibited with the 1D example (snap-backs), a monotonous increase of the load does not allow to capture the solution, so that specific arc-length techniques have to be applied, see for instance Lorentz and Badel (2003). This is a quite classical feature of brittle behavior. The results are presented in figure XI.4 in terms of the damage distribution. Two conclusions can be drawn:

- The damage concentrates in a band of width equal to the size of a single finite element, as already noticed in the 1D example. As the total energy dissipated by the structure is proportional to the area of the damaged zone, it also depends on the mesh size: the finer the mesh, the smaller the dissipated energy. This is unacceptable. Worse, if the size of the finite elements goes to zero, so does the energy: the computation would predict a fracture of the specimen without dissipation, as in the rod case.
- The orientation of the band is not controlled by the loading mode, as would have been expected (a mode I propagation, normal to the tensile direction). It is set by the mesh orientation. This is another aspect of spurious mesh-dependency. It should be noticed that the dependence on the mesh orientation appears as a severe limitation of solution strategies that set the mesh size as a material parameter to control the localization phenomenon since the numerical results are still not predictive.

Elasticity	Damage	
$E = 20$ GPa	$\sigma^y = 3$ MPa	$H = 5000$ MPa
$\nu = 0.2$	$k1.125\ 10^{-3}$ MPa	$\gamma = 0.25$

Table XI.1: Material parameters for the brittle law.

1.2 BIFURCATION MODES IN ELASTOPLASTIC SOLIDS

The formulation of the elastoplastic constitutive framework including one single inelastic mechanism is recalled first and used in the subsequent bifurcation analysis. For more elaborate plasticity models including multiple mechanisms of inelastic deformation, the reader is referred to Petryk (2000). The notions of uniqueness, stability and localization are presented briefly here. More details can be found in (Petryk, 1997; Besson et al., 2001a; Nguyen, 2002).

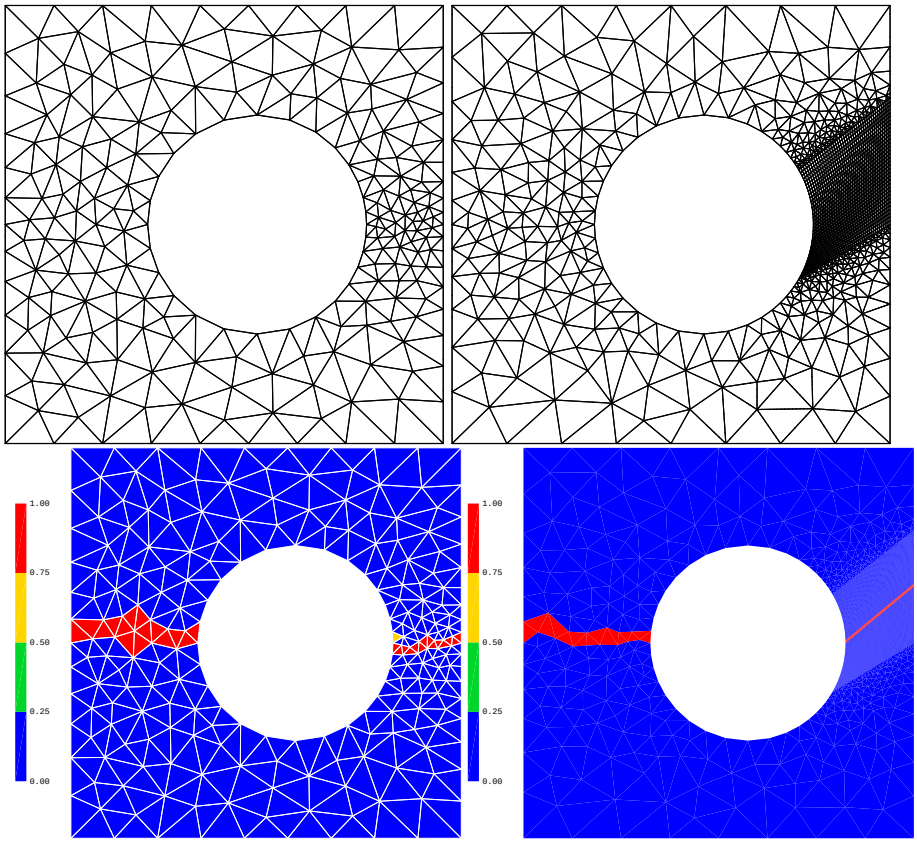

Figure XI.4: Two different spatial discretizations of the perforated plate: damage distribution

1.2.1 Formulation of the boundary value problem

Linear incremental formulation

Under small strain conditions, the total strain rate can be decomposed into an elastic and a plastic part

$$\dot{\underset{\sim}{\varepsilon}} = \dot{\underset{\sim}{\varepsilon}}^e + \dot{\underset{\sim}{\varepsilon}}^p \tag{12}$$

The constitutive behavior of an elastoplastic solid is then described by

- the elastic law
$$\underset{\sim}{\sigma} = \underset{\approx}{\mathbf{E}} : \underset{\sim}{\varepsilon}^e \tag{13}$$
where $\underset{\approx}{\mathbf{E}}$ is the four-rank elasticity tensor;
- the yield function $g(\underset{\sim}{\sigma}, \alpha)$, where α represents the set of hardening variables;
- the plastic flow rule
$$\dot{\underset{\sim}{\varepsilon}}^p = \dot{\lambda}\ \underset{\sim}{\mathbf{P}} \tag{14}$$
- the evolution equations of the hardening variables that are assumed to have the form
$$\dot{\alpha}\ =\ \dot{\lambda} h \tag{15}$$

The plastic loading condition reads

$$\dot{\lambda} > 0 \tag{16}$$

The consistency conditions are: $g = 0$ and $\dot{g} = 0$. It follows that

$$\dot{g} = \underset{\sim}{\mathbf{N}} : \dot{\underset{\sim}{\sigma}} - \dot{\lambda} H, \quad \text{with} \quad \underset{\sim}{\mathbf{N}} = \frac{\partial g}{\partial \underset{\sim}{\sigma}}, \quad H = -\frac{\partial g}{\partial \alpha}.h \tag{17}$$

where H is the hardening modulus. Non-associated plasticity, meaning that $\underset{\sim}{\mathbf{P}} \neq \underset{\sim}{\mathbf{N}}$, is taken into account. As a result

$$\dot{\lambda} = \frac{\underset{\sim}{\mathbf{N}} : \dot{\underset{\sim}{\sigma}}}{H} \tag{18}$$

If the material has a hardening behavior ($H > 0$), the plastic loading condition can be written as: $\underset{\sim}{\mathbf{N}} : \dot{\underset{\sim}{\sigma}} > 0$. This does not hold for strain-softening materials for which we must express the plastic loading conditions in terms of $\dot{\underset{\sim}{\varepsilon}}$ instead $\dot{\underset{\sim}{\sigma}}$. From (12), (13) and (17), we derive that

$$\dot{\lambda} = \frac{\underset{\sim}{\mathbf{N}} : \underset{\approx}{\mathbf{E}} : \dot{\underset{\sim}{\varepsilon}}}{H + \underset{\sim}{\mathbf{N}} : \underset{\approx}{\mathbf{E}} : \underset{\sim}{\mathbf{P}}} \tag{19}$$

Provided that

$$H + \underset{\sim}{\mathbf{N}} : \underset{\approx}{\mathbf{E}} : \underset{\sim}{\mathbf{P}} > 0 \tag{20}$$

(no “snap-back” behavior for the material point), the plastic loading condition (16) becomes

$$\underset{\sim}{\mathbf{N}} : \underset{\approx}{\mathbf{E}} : \dot{\underset{\sim}{\varepsilon}} > 0 \tag{21}$$

which is valid for softening materials as well as hardening ones. The constitutive equations take then the incremental form:

$$\dot{\underset{\sim}{\sigma}} = \underset{\approx}{\mathbf{L}} : \dot{\underset{\sim}{\varepsilon}} \tag{22}$$

where

$$\underset{\approx}{\mathbf{L}} = \underset{\approx}{\mathbf{E}} \quad \text{if} \quad g < 0 \quad \text{or} \quad (g = 0 \quad \text{and} \quad \underset{\sim}{\mathbf{N}} : \underset{\approx}{\mathbf{E}} : \dot{\underset{\sim}{\varepsilon}} \leq 0) \tag{23}$$

$$\underset{\approx}{\mathbf{L}} = \underset{\approx}{\mathbf{D}} \quad \text{if} \quad g = 0 \quad \text{and} \quad \underset{\sim}{\mathbf{N}} : \underset{\approx}{\mathbf{E}} : \dot{\underset{\sim}{\varepsilon}} > 0 \tag{24}$$

with

$$\underset{\approx}{\mathbf{D}} = \underset{\approx}{\mathbf{E}} - \frac{(\underset{\approx}{\mathbf{E}} : \underset{\sim}{\mathbf{P}}) \bigotimes (\underset{\sim}{\mathbf{N}} : \underset{\approx}{\mathbf{E}})}{H + \underset{\sim}{\mathbf{N}} : \underset{\approx}{\mathbf{E}} : \underset{\sim}{\mathbf{P}}} \tag{25}$$

Formulation of the rate problem

The solid domain is denoted Ω and its boundary $\partial\Omega$. $\partial\Omega$ is separated in two parts: $\partial_1\Omega$ where forces are prescribed and $\partial_2\Omega$ where displacements are prescribed ($\partial_1\Omega \cup \partial_2\Omega = \partial\Omega$ and $\partial_1\Omega \cap \partial_2\Omega = \varnothing$). For given fields of the rates of body forces $\dot{\vec{f}}$, surfaces forces $\dot{\vec{T}}$ on the part $\partial_1\Omega$ of the boundary of the domain Ω, and velocity $\vec{V}$ on $\partial_2\Omega$, the rate problem consists in finding the displacement rates $\vec{v}$ in Ω satisfying:

$$\begin{cases} \dot{\underset{\sim}{\varepsilon}} = \frac{1}{2}(\nabla\vec{v} + \nabla^t\vec{v}) \\ \text{div}\ \dot{\underset{\sim}{\sigma}} + \dot{\vec{f}} = 0, \quad \dot{\underset{\sim}{\sigma}} = \underset{\approx}{\mathbf{L}} : \dot{\underset{\sim}{\varepsilon}} \\ \dot{\underset{\sim}{\sigma}} \,.\, \vec{n} = \dot{\vec{T}} \quad \text{on} \quad \partial\Omega_1, \quad \vec{v} = \vec{V} \quad \text{on} \quad \partial\Omega_2 \end{cases} \tag{$\mathcal{P}$}$$

The problem $(\mathcal{P})$ is non-linear because of relations (23) and (24).

1.2.2 Loss of uniqueness; general bifurcation modes

Hill's condition

Let $(\dot{\underset{\sim}{\sigma}}_A, \dot{\underset{\sim}{\varepsilon}}_A)$ and $(\dot{\underset{\sim}{\sigma}}_B, \dot{\underset{\sim}{\varepsilon}}_B)$ be two distinct solutions of the boundary value problem for a continuous system and let us consider the differences $\Delta\,\dot{\underset{\sim}{\sigma}} = \dot{\underset{\sim}{\sigma}}_A - \dot{\underset{\sim}{\sigma}}_B$ and $\Delta\,\dot{\underset{\sim}{\varepsilon}} = \dot{\underset{\sim}{\varepsilon}}_A - \dot{\underset{\sim}{\varepsilon}}_B$. The associated velocity field $\Delta\vec{v}$ vanishes on the part of the boundary of the solid Ω where the velocity is prescribed and is therefore a kinematically admissible velocity field in the expression of the principle of virtual power. Applying the principle of virtual power successively to solutions A and B on body Ω, Hill (cf. Hill (1958)) gets a necessary condition for loss of uniqueness:

$$\int_\Omega \Delta\,\dot{\underset{\sim}{\sigma}} : \Delta\,\dot{\underset{\sim}{\varepsilon}}\, dV = 0 \tag{26}$$

A local sufficient condition for uniqueness (in fact for the linear comparison solid) is then

$$\dot{\underset{\sim}{\sigma}} : \dot{\underset{\sim}{\varepsilon}} \ > \ 0 \tag{27}$$

for all kinematically admissible velocity fields. This condition is called positiveness of the local second-order work. When a linear incremental formulation of the constitutive

equations like (22) exists, the positiveness of the local second-order work is equivalent to the definite positiveness of the four-rank tensor $\underset{\approx}{\mathbf{D}}^s$, where s denotes symmetrization ($D^s_{ijkl} = (D_{ijkl} + D_{klij})/2$). A necessary condition for the local loss of uniqueness is then

$$\det\ \underset{\approx}{\mathbf{D}}^s = 0 \tag{28}$$

When uniqueness is lost, general bifurcation modes (like necking ...) become possible. These modes can be diffuse or localized deformation modes. However bifurcation modes associated with strain rate jumps at the boundary of the bifurcated zone may occur only later. The corresponding bifurcation criteria will be derived in section 1.2.3.

General bifurcation modes in non-associated elastoplasticity

A spectral analysis of the elastoplastic tangent tensors $\underset{\approx}{\mathbf{D}}$ and $\underset{\approx}{\mathbf{D}}^s$ is necessary in order to obtain explicit criteria for the possible loss of uniqueness and the associated bifurcation modes. $\underset{\approx}{\mathbf{D}}^s$ has six symmetric eigentensors Neilsen and Schreyer (1993). This amounts to solving the system of equations

$$\underset{\approx}{\mathbf{D}}^s : \underset{\sim}{\mathbf{x}} = \omega\ \underset{\sim}{\mathbf{x}} \tag{29}$$

The determinant of this homogeneous system must be zero if non-trivial solutions x_{ij} are to be found. This condition gives a relation between the hardening modulus and ω. The critical hardening modulus H^u associated with possible loss of uniqueness, is then obtained for $\omega = 0$. The complete analysis has been carried out by Raniecki and Bruhns (1981) and Runesson and Mróz (1989). They give the following sufficient condition for uniqueness

$$H > H^u = \frac{1}{2}(\sqrt{\underset{\sim}{\mathbf{N}} : \underset{\approx}{\mathbf{E}} : \underset{\sim}{\mathbf{N}}}\sqrt{\underset{\sim}{\mathbf{P}} : \underset{\approx}{\mathbf{E}} : \underset{\sim}{\mathbf{P}}} - \underset{\sim}{\mathbf{N}} : \underset{\approx}{\mathbf{E}} : \underset{\sim}{\mathbf{P}}) \tag{30}$$

The fundamental bifurcation mode is

$$\underset{\sim}{\mathbf{x}} = \frac{\underset{\sim}{\mathbf{P}}}{\sqrt{\underset{\sim}{\mathbf{P}} : \underset{\approx}{\mathbf{E}} : \underset{\sim}{\mathbf{P}}}} + \frac{\underset{\sim}{\mathbf{N}}}{\sqrt{\underset{\sim}{\mathbf{N}} : \underset{\approx}{\mathbf{E}} : \underset{\sim}{\mathbf{N}}}} \tag{31}$$

For associated plasticity $\underset{\sim}{\mathbf{P}} = \underset{\sim}{\mathbf{N}}$ and the critical hardening modulus is then

$$H^u = 0 \tag{32}$$

Well-posedness of the rate boundary value problem for the linear comparison solid

The linear comparison solid introduced in Hill (1958) is obtained when unloading is excluded, so that

$$\underset{\approx}{\mathbf{L}} = \underset{\approx}{\mathbf{D}} \tag{33}$$

In that linear case, necessary and sufficient conditions can be worked out for the well-posedness of the rate problem. Following Benallal et al. (1989), the rate boundary problem is said to be well-posed if it admits a finite number of linearly independent solutions which depend continuously on the data, and which constitute diffuse modes of deformation. The linear rate problem for a solid with boundary and possible interfaces is then well-posed if and only if the following conditions are met:

(i) the ellipticity condition;
(ii) the boundary complementing condition;
(iii) the interfacial complementing condition.

Condition (i) states that the rate equilibrium equations must remain an elliptic set of partial differential equations in the body Ω. The condition (ii) deals with possible bifurcation close to the boundary of Ω. In that case the boundary conditions must be fulfilled and represent therefore an additional or *complementing* condition. In the case of bifurcation close to an interface separating two materials, the compatibility and equilibrium requirements at the interface must be taken into account. This corresponds to the additional condition (iii). The conditions (i) to (iii) can be shown to be equivalent to the follwing ones Besson et al. (2001a):

$(i)'$ $\det \quad \vec{n}.\underset{\approx}{\mathbf{D}}.\vec{n} \neq 0 \quad \forall \vec{n} \neq 0 \quad \text{and} \quad \forall M \in \overline{\Omega}$;
$(i)''$ bifurcation modes involving jumps of the velocity gradient are precluded;
$(i)'''$ stationary acceleration waves are precluded.

The meaning of conditions $(i)'$, $(i)''$ and $(i)'''$ will be given in the next section. The equivalence between $(i)'$ and $(i)''$ is established for instance in Ottosen and Runesson (1991b). The link between the existence of discontinuous bifurcation modes and of stationary acceleration waves has been seen by Mandel (cf. Mandel (1966) and section 1.2.3) and is summarized in Ottosen and Runesson (1991a).

The boundary value problem written for finite bodies can become ill-posed while the incremental field equations remain elliptic, as a consequence of the failure of the complementary condition at the boundaries or interfaces. The failure of the boundary complementing condition is equivalent to the existence of *Rayleigh surface waves*. This can be investigated by looking for wave solutions:

$$\vec{v} = \vec{w} \exp(i\vec{k}.\vec{x}) \tag{34}$$

Body waves correspond to solutions with real components of $\vec{k}$. If the solid extends over the half-space $x_1 \geq 0$, the boundary being free of traction, solutions with k_1 complex leading to Rayleigh free surface waves, will decay exponentially into the body, according to Needleman and Ortiz (1991), if:

$$\Im m\, k_1 \geq 0 \tag{35}$$

Similar conditions exist for the existence of *Stoneley stationary interfacial waves*, that are deformation modes localized at each side of an interface. The interface can be perfect or described by a constitutive equation like in Suo et al. (1992).

If no length scales are introduced in the constitutive equations, the wave length of body, surface or interfacial waves, remains arbitrary. The mismatch in mechanical properties at an interface can induce stress and strain concentrations that may act as initiation sites for localization. Conversely, grain boundaries can act as barriers to localization that originates in the bulk of the material.

1.2.3 Existence of velocity gradient discontinuities

Acceleration waves; acoustic tensor

Following Mandel (1962) and Ottosen and Runesson (1991a), we investigate the possibility of emergence of deformation modes involving jumps of the acceleration,

of the velocity gradient and of the stress rate across a moving surface S with normal $\vec{n}$ (where $[\![\cdot]\!]$ denotes a jump across the interface):

$$[\![\vec{\dot{u}}]\!] \neq \vec{0}, \quad [\![\nabla\vec{\dot{u}}]\!] \neq \underset{\sim}{\mathbf{0}} \quad \text{and} \quad [\![\underset{\sim}{\dot{\sigma}}]\!] \neq \underset{\sim}{\mathbf{0}} \tag{36}$$

The symbol $[\![f]\!]$ denotes the difference between the values taken by f on both sides of the surface S. But it is assumed that

$$[\![\vec{u}]\!] = [\![\dot{\vec{u}}]\!] = 0 \quad \text{and} \quad [\![\underset{\sim}{\sigma}]\!] = 0 \tag{37}$$

The discontinuity surface, S, propagates with the normal speed $U = \dot{\vec{x}}.\vec{n}$ where $\vec{x} \in S$. According to Hadamard's compatibility conditions, the jump of the velocity gradient at the interface must have the form

$$\exists \vec{g} / \; [\![\nabla\vec{\dot{u}}]\!] = \vec{g} \otimes \vec{n} \tag{38}$$

A detailed description of singular surfaces can be found in Truesdell and Toupin (1960) and Thomas (1961). Similarly

$$\exists \, \underset{\sim}{\mathbf{g}} / \; [\![\nabla \, \underset{\sim}{\sigma}]\!] = \underset{\sim}{\mathbf{g}} \otimes \vec{n} \tag{39}$$

Furthermore the conditions (37) must hold at each time t, so that

$$[\![\vec{\dot{u}}]\!] + U\vec{g} = \vec{0}, \quad [\![\underset{\sim}{\dot{\sigma}}]\!] + U \, \underset{\sim}{\mathbf{g}} = \underset{\sim}{\mathbf{0}} \tag{40}$$

Applying the previous relation to vector $\vec{n}$, one gets

$$[\![\underset{\sim}{\dot{\sigma}}]\!].\vec{n} + U[\![\text{div } \underset{\sim}{\sigma}]\!] = \vec{0} \tag{41}$$

On the other hand, continuing equilibrium implies

$$[\![\text{div } \underset{\sim}{\sigma}]\!] = \rho[\![\vec{\dot{u}}]\!] \tag{42}$$

provided that the body forces are the same on each side of S. Combining the two last equations gives

$$[\![\underset{\sim}{\dot{\sigma}}]\!].\vec{n} = \rho U^2 \vec{g} \tag{43}$$

If the constitutive equations have the linear incremental form (22), and assuming that $[\![\underset{\approx}{\mathbf{L}}]\!] = 0$, one gets

$$\underset{\sim}{\mathbf{Q}} .\vec{g} = \rho U^2 \vec{g} \tag{44}$$

where

$$Q_{ij} = n_k D_{iklj} n_l \tag{45}$$

under plastic loading conditions on each side of S. $\underset{\sim}{\mathbf{Q}}$ is called the acoustic tensor. The previous relation will be written

$$\underset{\sim}{\mathbf{Q}} = \vec{n}. \underset{\approx}{\mathbf{D}}.\vec{n} \tag{46}$$

in the sequel. As a result, the existence of discontinuity surfaces of the type (36) depends on the solutions of the eigenvalue problem (44). The above assumption $[\![\underset{\approx}{\mathbf{L}}]\!] = 0$ is met when one starts from a homogeneous solution and one investigates the occurrence of a possible bifurcation mode. Before a bifurcated solution develops on one side of S, the tangent moduli of the material points on both sides of S coincide.

Discontinuous bifurcation modes in the static case

We consider now the following jump conditions across a surface S which is not moving

$$[\![\nabla \dot{\vec{u}}]\!] \neq \underset{\sim}{0} \text{ and } [\![\dot{\vec{u}}]\!] = \mathrm{C}^{\mathrm{st}} \tag{47}$$

Condition (38) must still hold and we make use of the linear incremental form (22). We investigate plastic/plastic bifurcations for which $[\![\underset{\approx}{\mathbf{L}}]\!] = 0$. Elastic/plastic bifurcation modes will be considered in the next section. The equilibrium condition at the surface S reads in the static case

$$[\![\dot{\underset{\sim}{\sigma}}]\!] .\vec{n} = \vec{0} \tag{48}$$

Combining (38) and (48) leads to the condition

$$\underset{\sim}{\mathbf{Q}} . \vec{g} = \vec{0} \tag{49}$$

where the acoustic tensor is still defined by (45). Non trivial solutions require the acoustic tensor to become singular. These discontinuous bifurcation modes can be regarded as stationary plastic waves.

The general character of the governing partial differential equations and its dependency on the current value of the stress and tangent moduli is investigated in Hill and Hutchinson (1975). Ellipticity can be lost and bifurcation modes may then develop. There is an equivalence between the *loss of ellipticity* of the governing equations and the existence of discontinuous bifurcation modes.

Conditions for plastic/plastic and elastic/plastic bifurcations

If plastic loading occurs on each side of S, the bifurcation modes are called plastic/plastic localization modes. Necessary and sufficient conditions for such modes to become possible inside the body have been worked out by Rice (1976):

$$\det \quad \underset{\sim}{\mathbf{Q}} = \det \quad \vec{n}.\underset{\approx}{\mathbf{D}}.\vec{n} = 0 \quad \text{and} \quad \vec{n}.\underset{\approx}{\mathbf{E}} : \underset{\sim}{\mathbf{P}} \neq \vec{0} \tag{50}$$

If elastic unloading occurs on one side of S, the associated bifurcation modes are called elastic/plastic localization modes. A necessary and sufficient condition for the onset of elastic/plastic localization modes inside the body is:

$$\det \quad \underset{\sim}{\mathbf{Q}} = \det \quad \vec{n}.\underset{\approx}{\mathbf{D}}.\vec{n} < 0 \quad \text{and} \quad \vec{n}.\underset{\approx}{\mathbf{E}} : \underset{\sim}{\mathbf{P}} \neq \vec{0} \tag{51}$$

It means that in the case of usual elastoplastic materials for which the work-hardening rate decreases with strain, an elastic/plastic localization mode involving elastic unloading cannot occur before the condition for plastic/plastic bifurcation modes (50) is fulfilled. However it does not exclude the fact that elastic unloading occurs on one side just after plastic/plastic bifurcation.

The reader is referred to Benallal et al. (1989) for bifurcation conditions for a discontinuity surface S to appear at or to reach the boundary of a solid.

1.2.4 Bifurcation analysis in elastoplasticity

Critical hardening modulus for a given normal $\vec{n}$

Rice has determined the critical hardening modulus for which a plastic/plastic bifurcation becomes possible across a surface S of given normal $\vec{n}$. One starts from the

equilibrium equation at the interface

$$\underset{\approx}{\mathbf{D}} : [\![\dot{\underset{\approx}{\varepsilon}}]\!] .\vec{n} = \vec{0} \tag{52}$$

where the linear incremental form (22) has been used. Taking (38) and (25) into account, one obtains

$$\left(\vec{n}.\underset{\approx}{\mathbf{E}}.\vec{n} \; - \; \frac{1}{A} (\vec{n}.\underset{\approx}{\mathbf{E}} : \underset{\sim}{\mathbf{P}}) \otimes (\underset{\sim}{\mathbf{N}} : \underset{\approx}{\mathbf{E}}.\vec{n}) \right) .\vec{g} = \vec{0}, \quad A = H + \underset{\sim}{\mathbf{N}} : \underset{\approx}{\mathbf{E}} : \underset{\sim}{\mathbf{P}} \tag{53}$$

It can be checked that

$$H(\vec{n}) = - \underset{\sim}{\mathbf{N}} : \underset{\approx}{\mathbf{E}} : \underset{\sim}{\mathbf{P}} + (\underset{\sim}{\mathbf{N}} : \underset{\approx}{\mathbf{E}}.\vec{n}).(\vec{n}.\underset{\approx}{\mathbf{E}}.\vec{n})^{-1}.(\vec{n}.\underset{\approx}{\mathbf{E}} : \underset{\sim}{\mathbf{P}}) \tag{54}$$

$$\vec{g} \propto (\vec{n}.\underset{\approx}{\mathbf{E}}.\vec{n})^{-1}.(\vec{n}.\underset{\approx}{\mathbf{E}} : \underset{\sim}{\mathbf{P}}) \tag{55}$$

are solutions of the previous equations. The uniqueness of this solution is proved in (Ottosen and Runesson, 1991b; Besson et al., 2001a) who investigated both plastic/plastic and elastic/plastic bifurcation modes.

Critical hardening modulus and orientation of the first possible shear band

For materials with decreasing hardening modulus, the critical hardening modulus for which the first discontinuous bifurcation mode becomes possible is:

$$H^{cr} = \max_{\|\vec{n}\|=1} \quad H(\vec{n}) \tag{56}$$

where $H(\vec{n})$ is given by equation (54).

The orientation of the first possible band of localized deformation is given by the values of $\vec{n}$ for which H^{cr} is reached.

Three-dimensional case

The problem reduces to maximizing the Lagrangian function:

$$L(\vec{n}, \lambda) = H(\vec{n}) - \lambda(\|\vec{n}\|^2 - 1). \tag{57}$$

For isotropic elasticity,

$$H(\vec{n}) = 2\mu(2(\vec{n}.\underset{\sim}{\mathbf{P}}).(\underset{\sim}{\mathbf{N}}.\vec{n}) - (\vec{n}.\underset{\sim}{\mathbf{P}}.\vec{n})(\vec{n}.\underset{\sim}{\mathbf{N}}.\vec{n}) - \underset{\sim}{\mathbf{P}} : \underset{\sim}{\mathbf{N}}$$

$$- \frac{\nu}{1-\nu} (\vec{n}.\underset{\sim}{\mathbf{P}}.\vec{n} - \text{trace}\underset{\sim}{\mathbf{P}})(\vec{n}.\underset{\sim}{\mathbf{N}}.\vec{n} - \text{trace}\underset{\sim}{\mathbf{N}})) \tag{58}$$

The associated vector $\vec{g}$ is

$$\vec{g} = 2\,\underset{\sim}{\mathbf{P}}.\vec{n} - \frac{1}{1-\nu} (\vec{n}.\underset{\sim}{\mathbf{P}}.\vec{n})(\vec{n}.\underset{\sim}{\mathbf{N}}.\vec{n})\;\vec{n} + \frac{\nu}{1-\nu} (\text{trace}\underset{\sim}{\mathbf{P}})\;\vec{n} \tag{59}$$

We refer to the method developed in Bigoni and Hueckel (1991) to solve this maximization problem for general non-associated elastoplasticity. But the present analysis is restricted to associated plasticity: $\underset{\sim}{\mathbf{P}} = \underset{\sim}{\mathbf{N}}$. Furthermore, in this subsection,

incompressible behavior is considered for simplicity: $\text{trace}\,\underset{\sim}{\mathbf{P}} = 0$. Equation (57) combined with (54) and written in the principal axes of $\underset{\sim}{\mathbf{P}}$ then becomes:

$$L(\vec{n},\lambda) = 2\mu\left(2\,n_i^2P_i^2 \;-\; \sum_{i=1}^{3} P_i^2 \;-\; \frac{1}{1-\nu}\,(n_i^2P_i)^2\right) \;-\; \lambda(\sum_{i=1}^{3} n_i^2 - 1) \quad (60)$$

Writing $\dfrac{\partial L}{\partial \lambda} = 0$ and $\dfrac{\partial L}{\partial n_k} = 0$ makes the problem equivalent to the resolution of the system:

$$n_k\left(P_k^2 \;-\; \frac{1}{1-\nu}\,(n_i^2P_i)P_k \;-\frac{\lambda}{4\mu}\right) = 0 \quad k \in \Big\{1,2,3\Big\} \text{ no sum on } k \qquad (61)$$

If $n_1n_2n_3 \neq 0$, the system is indeterminate or impossible depending on P_1, P_2, P_3.

If $n_k = 0$ and $n_in_j \neq 0$ (i, j, k distinct),:

- if $P_i = P_j$, the system is indeterminate;
- if $P_i \neq P_j$,

$$n_i^2 = \frac{P_i + \nu P_k}{P_i - P_j} \quad \text{and} \quad n_j^2 = 1 - n_i^2 \qquad (62)$$

The jump of the strain rate across the surface of normal $\vec{n}$ is also described by $\vec{g}$:

$$\begin{cases} g_i = (P_i - P_j)\,n_i \\ g_j = (P_j - P_i)\,n_j \\ g_k = 0 \end{cases} \quad , \quad \begin{cases} [\![\,\dot{\underset{\sim}{\varepsilon}}_i\,]\!] = P_i + \nu P_k \\ [\![\,\dot{\underset{\sim}{\varepsilon}}_j\,]\!] = P_j + \nu P_k \\ [\![\,\dot{\underset{\sim}{\varepsilon}}_k\,]\!] = 0 \end{cases}$$

the corresponding critical hardening modulus being

$$H^{cr} = -EP_k^2 \qquad (63)$$

If $n_i^2 = 1$ and $n_j = n_k = 0$,

$$H^{cr} = -2\mu\left(\frac{(P_j + \nu P_k)^2}{1-\nu} + (1+\nu)P_k^2\right) \qquad (64)$$

The first possible band is given by the combination i, j, k for which H^{cr} has the highest value. Note therefore that theoretically, for the 3–dimensional solid, a negative modulus H does not necessarily mean localization.

Two-dimensional case

The plane strain case can be solved using the three-dimensional analysis. If the deformation plane is normal to direction 3

$$\dot{\varepsilon}_{33} = \dot{\varepsilon}^e_{33} + \dot{\varepsilon}^p_{33} \qquad (65)$$

If plastic flow is large enough and assuming that the elastic strain remains small enough, the contribution $\dot{\varepsilon}^p_{33}$ can be neglected. Furthermore the direction 3 is supposed

to be a principal direction of $\underset{\sim}{\mathbf{P}}$. As a result, we have almost $P_3 = 0$ so that (63) becomes

$$H^{\text{plane strain}} = 0 \tag{66}$$

We have also $P_1 + P_2 = 0$, so that (62) gives

$$n_1^2 = n_2^2 = \frac{1}{2} \tag{67}$$

The orientation of shear bands under plane strain conditions is 45°.

The plane stress case must be reexamined. The solid is considered two-dimensional. This means for instance that the compatibility condition in the third direction will not be ensured. The condition $\varepsilon_{33,12} = 0$ holds only if ε_{33} is linear in x_1 and x_2. The vectors $\vec{g}$ and $\vec{n}$ are supposed to lie in the 1–2 plane. Lastly the elasticity matrix in the isotropic case takes a special form

$$\begin{bmatrix} \sigma_{11} \\ \sigma_{22} \\ \sigma_{12} \end{bmatrix} = \frac{2\mu}{1-\nu} \begin{bmatrix} 1 & \nu & 0 \\ \nu & 1 & 0 \\ 0 & 0 & 1-\nu \end{bmatrix} \begin{bmatrix} \varepsilon_{11}^e \\ \varepsilon_{22}^e \\ \varepsilon_{12}^e \end{bmatrix} \tag{68}$$

In that conditions, the critical hardening modulus for a given orientation $\vec{n}$ is

$$\begin{aligned} H^{\text{plane stress}}(\vec{n}) &= 2\mu(2(\vec{n}.\underset{\sim}{\mathbf{P}}).(\underset{\sim}{\mathbf{N}}.\vec{n}) - (\vec{n}.\underset{\sim}{\mathbf{P}}.\vec{n})(\vec{n}.\underset{\sim}{\mathbf{N}}.\vec{n}) \\ &- \underset{\sim}{\mathbf{P}} : \underset{\sim}{\mathbf{N}} - \nu(\vec{n}.\underset{\sim}{\mathbf{P}}.\vec{n} - \text{trace}\underset{\sim}{\mathbf{P}})(\vec{n}.\underset{\sim}{\mathbf{N}}.\vec{n} - \text{trace}\underset{\sim}{\mathbf{N}})) \end{aligned} \tag{69}$$

where $\vec{n} = [n_1\ n_2]^t$ and $\underset{\sim}{\mathbf{P}}$ and $\underset{\sim}{\mathbf{Q}}$ are also two-dimensional, and $\vec{g}$ is given by:

$$\vec{g} = 2\,\underset{\sim}{\mathbf{P}}.\vec{n} - (1+\nu)(\vec{n}.\underset{\sim}{\mathbf{P}}.\vec{n})\ \vec{n} + \nu(\text{trace}\underset{\sim}{\mathbf{P}})\vec{n} \tag{70}$$

$$H(\vec{n}) = 2\mu\left(2P_i^2 n_i^2 - (P_i n_i^2)^2 - \sum_{i=1}^{2} P_i^2 - \nu(n_i^2 P_i - \sum_{i=1}^{2} P_i)^2\right) \tag{71}$$

$$\frac{\partial H}{\partial n_1^2} = -4\mu(1+\nu)(P_1 - P_2)(n_1^2 P_1 + n_2^2 P_2 - P_1 - P_2) \tag{72}$$

If $P_1 = P_2, H^{cr} = -2\mu(1+\nu)P_1^2$ and $\vec{n}$ is arbitrary,
If $P_1 \neq P_2$,

$$n_1^2 = \frac{P_1}{P_1 - P_2}, \quad n_2^2 = 1 - n_1^2 \tag{73}$$

$$g_1 = (P_1 - P_2)n_1, \quad g_2 = -(P_1 - P_2)n_2 \tag{74}$$

and

$$H^{\text{plane stress}} = 0 \tag{75}$$

The jump is then proportional to $[\![\dot{\varepsilon}_1]\!] = P_1$ and $[\![\dot{\varepsilon}_2]\!] = P_2$. The calculation proves that for plane stress also, the critical hardening modulus for discontinuous bifurcations is generally zero.

The two-dimensional solid is therefore more prone to localization than the real solid. The reason is that some bifurcation modes though incompatible (in the sense of Hadamard) in the direction 3 are compatible in the plane 1-2 and are then full discontinuous bifurcation modes for the 2D solid.

1.2.5 Stability

Concerning stability we present Mandel's approach (Mandel, 1966). A more general framework can be found in (Nguyen, 2002). Let us consider a solid in a state of equilibrium. Perturbations of the equilibrium may be represented by plane waves in direction $\vec{g}$

$$\vec{u}^\star = f(\vec{n}.\vec{x} \pm Ut)\ \vec{g} \tag{76}$$

One assumes that the initial equilibrium stress $\underset{\sim}{\sigma}$ is homogeneous. $\underset{\sim}{\sigma}^\star$ denotes then the stress variation due to the perturbation. It follows that

$$\text{div}\ \underset{\sim}{\sigma}^\star = \rho\ \ddot{\vec{u}}^\star \tag{77}$$

Furthermore it is assumed that the constitutive equations take the linear incremental form (22) and that $\underset{\approx}{\mathbf{D}}$ is initially homogeneous and that it remains constant around the equilibrium state. Under these conditions and taking (76) into account, the last equation becomes

$$D_{ijkl}\ u_{k,lj} = \ddot{u}_i, \quad n_i\ D_{ijkl}\ n_l c_k = \rho U^2\ c_i \tag{78}$$

that is

$$\underset{\sim}{\mathbf{Q}}\ .\ \vec{g} = \rho U^2\ \ \vec{g} \tag{79}$$

As a result plane waves and acceleration waves are governed by the same equations (compare (44) and (79)), even though they represent two distinct phenomena. The assumptions in the previous calculation correspond to the so-called "acoustic approximation" in fluid mechanics, which explains the denomination of tensor $\underset{\sim}{\mathbf{Q}}$. When the eigenvalues of the acoustic tensor are real and positive, equilibrium is said to be stable because plane waves can propagate without growing. If they are real but negative, equilibrium is unstable with divergence. Complex eigenvalues with negative real part lead to a phenomenon called *flutter instability* in aerodynamics.

1.2.6 Localization criteria

The various bifurcation criteria that have been established in the previous sections are summed up on figure XI.5. Two critical hardening moduli have been defined: H^u corresponds to possible loss of uniqueness and H^{cr} is associated with the possible existence of discontinuous bifurcation modes. An additional critical hardening modulus can be determined for which general bifurcation modes become compatible, i.e. are of the form $[\![\ \dot{\underset{\sim}{\varepsilon}}\ ]\!] = (\vec{g} \otimes \vec{n}\ +\ \vec{n} \otimes \vec{g})/2$

$$\dot{\underset{\sim}{\varepsilon}} : \underset{\approx}{\mathbf{D}} : \dot{\underset{\sim}{\varepsilon}} = 0\ \Rightarrow\ \vec{g}.\underset{\sim}{\mathbf{Q}}.\vec{g} = \vec{g}.\underset{\sim}{\mathbf{Q}}^s.\vec{g} = 0 \tag{80}$$

which corresponds to the loss of positive definitiveness of the symmetrized acoustic tensor $\underset{\sim}{\mathbf{Q}}^s$. This condition is called loss of strong ellipticity. It happens for the critical value $H = H^{se}$. The physical meaning is the existence of compatible general bifurcation modes, which however do not necessarily fulfill equilibrium jump conditions.

In the general case, the sign of the three critical hardening moduli can be positive or negative. In particular bifurcation may occur while the material is hardening. In contrast, for associated plasticity at small strains, $H^u = 0$ so that bifurcations are

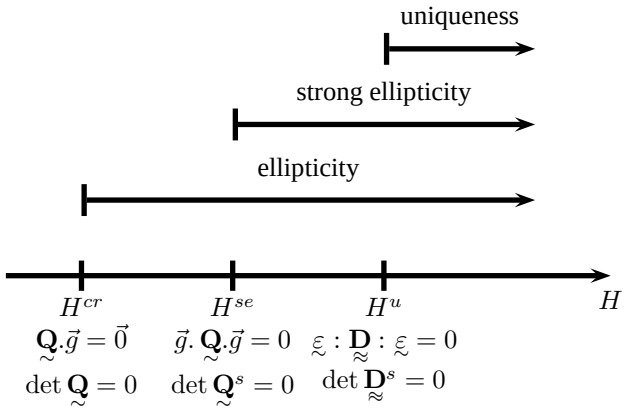

Figure XI.5: Bifurcation criteria in non-associated plasticity.

possible only for ideal plastic or strain-softening materials. Furthermore $\underset{\approx}{\mathbf{D}}$ and $\underset{\sim}{\mathbf{Q}}$ are then symmetric tensors so that $H^{se} = H^{cr}$.

In general, bifurcation may occur before the extremum $\dot{\underset{\sim}{\sigma}} = 0$ of the loading curve. The associated hardening modulus H^l for which $\det \underset{\approx}{\mathbf{D}} = 0$ corresponds to a limit point.

General bifurcation modes may induce diffuse or localized deformation. It is difficult in practice to distinguish between localized general bifurcations and discontinuous ones (shear bands strictly speaking). However one can assume that a general bifurcation which is also compatible in the sense of Hadamard will induce localized rather than diffuse deformation. That is why one may think of the strong ellipticity criterion as a good criterion for localization of deformation.

1.3 APPLICATION TO TENSILE TESTS IN ISOTROPIC INCOMPRESSIBLE AND COMPRESSIBLE ASSOCIATED ELASTOPLASTIC MATERIALS

1.3.1 J_2–theory: tensile test

We consider the example of an elastoplastic model with the von Mises criterion

$$g = J_2(\underset{\sim}{\sigma}) - R \ \text{ with } \ J_2(\underset{\sim}{\sigma}) = \sqrt{\frac{3}{2}\,\underset{\sim}{\sigma}^{dev} : \underset{\sim}{\sigma}^{dev}} \tag{81}$$

$\underset{\sim}{\sigma}^{dev}$ denoting the deviatoric part of $\underset{\sim}{\sigma}$. In that case,

$$\underset{\approx}{\mathbf{D}} = \underset{\approx}{\mathbf{E}} - \frac{2\mu^2}{H/3+\mu}\,\frac{\underset{\sim}{\sigma}^{dev} \otimes \underset{\sim}{\sigma}^{dev}}{\underset{\sim}{\sigma}^{dev} : \underset{\sim}{\sigma}^{dev}} \tag{82}$$

For isotropic elasticity, $\underset{\sim}{\mathbf{1}}$ is an eigentensor of $\underset{\approx}{\mathbf{D}}$ and the associated eigenvalue is $3k$ [1].

$$\underset{\sim}{\mathbf{d}}_1 = \frac{\underset{\sim}{\sigma}^{dev}}{\sqrt{\underset{\sim}{\sigma}^{dev} : \underset{\sim}{\sigma}^{dev}}} \tag{83}$$

[1] k: compressibility modulus, μ: shear modulus

is an eigentensor for the eigenvalue $\omega_1 = 2\mu H/(H+3\mu)$. The remaining eigentensors are in $\{\underset{\sim}{\mathbf{1}}, \underset{\sim}{s}^{dev}\}^{\perp}$ and the eigenvalue is 2μ. Accordingly, only one eigenvalue depends on the hardening modulus. Uniqueness is lost for $\omega_1 = 0 = H^u$. For tensile straining

$$[\underset{\sim}{\mathbf{d}}_1] = \frac{1}{\sqrt{6}} \begin{bmatrix} -1 & 0 & 0 \\ 0 & 2 & 0 \\ 0 & 0 & -1 \end{bmatrix} \tag{84}$$

This is an incompatible diffuse mode that gives rise to the necking phenomenon.

We restrict ourselves to the tension of a plate to study the bifurcation modes in the plane 1-2. The mode (84) is assumed to occur within a band of normal $\vec{n}$. The components of $\underset{\sim}{\mathbf{d}}_1$ in the basis $(\vec{m}, \vec{n})$ read:

$$[\underset{\sim}{\mathbf{d}}_1] = \frac{1}{\sqrt{6}} \begin{bmatrix} 2\sin^2\theta - \cos^2\theta & 3\cos\theta\sin\theta & 0 \\ 3\cos\theta\sin\theta & 2\cos^2\theta - \sin^2\theta & 0 \\ 0 & 0 & -1 \end{bmatrix} \tag{85}$$

This bifurcation mode becomes compatible in the sense of Hadamard in the 1-2 plane if it takes the form

$$\frac{1}{2}(\vec{g}\otimes\vec{n} + \vec{n}\otimes\vec{g})_{1-2\,plane} = \begin{bmatrix} 0 & g_1/2 \\ g_1/2 & g_2 \end{bmatrix} \tag{86}$$

in the $(\vec{m}, \vec{n})$ basis. This expression must be compared to the 2x2 submatrix in (85). Such a form is therefore obtained for

$$2\sin^2\theta - \cos^2\theta = 0, \;\; \tan^2\theta = \frac{1}{2}, \;\; \theta = \pm 35.26^\circ \tag{87}$$

It means that deformation can localize within a band with the previous orientation (see figure XI.6). However, compatibility is not ensured in the third direction until the critical hardening modulus for discontinuous bifurcations is reached

$$H^{cr} = -E/4 \tag{88}$$

according to equation (63). But the orientation of the band is then, according to equation (62)

$$n_1^2 = \frac{1+\nu}{3} \tag{89}$$

which gives $\theta = 42^\circ$ for $\nu = 0.33$.

These localization modes can be simulated using the finite element method in the 2D and 3D cases. We consider the tension of a plate with a geometrical or material imperfection. The mesh corresponds to one quarter of the entire plate. A thickness heterogeneity or a slightly lower yield strength are introduced according to trigger strain localization. A classical phenomenological elastoplastic model has been chosen involving isotropic hardening (Besson et al., 2001a). The hardening parameters are such that the material first hardens and then softens. The maximum is reached after small deformation. In the two-dimensional case, we use quadratic elements with eight nodes and nine integration points. In the three-dimensional case, we use 20-node bricks with 27 Gauss points.

In the 2D plane stress case, slightly after the maximum, the load-displacement curve displays an abrupt load drop and strain localizes within two narrow shear bands.

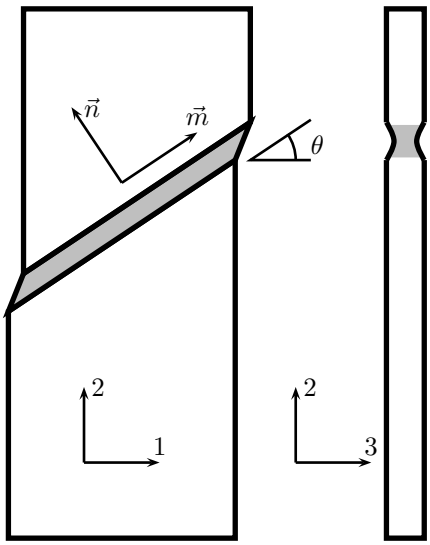

Figure XI.6: Shear band under tensile loading compatible in the plane and necking within the thickness.

Their orientation is, as predicted, 54.7° with respect to the tensile axis. The bands can be seen in figure XI.7, with two different meshes.

The plate is now a three-dimensional solid and has a one-element thickness. Elements are 20-nod bricks with 27 Gauss points. Once again shear bands appear in a softening material with the same orientation but the bands are much larger and strain in them much lower than for the 2D plate (figure XI.7). The reason is that the observed localization mode is only partially compatible. It is compatible in the plane 1-3 but the incompatibility in direction 2 results in necking. That is why we obtain a more diffuse strain field.

1.3.2 Elliptic potential

One of the most simple yield functions for compressible elastoplastic materials is the elliptic potential defined as (see also chapter VIII):

$$g(\underset{\sim}{\sigma}) = \sigma_\star - R, \quad \sigma_\star^2 = \frac{3}{2} C\, \underset{\sim}{\sigma}^{\rm dev} : \underset{\sim}{\sigma}^{\rm dev} + F(\text{trace } \underset{\sim}{\sigma})^2 \tag{90}$$

where C and F are material parameters, possibly depending on material porosity f, and R the hardening function. The tensor giving at each instant the direction of plastic flow is

$$\underset{\sim}{\mathbf{N}} = \frac{\partial g}{\partial\, \underset{\sim}{\sigma}} = \frac{1}{\sigma_\star} \left(\frac{3}{2} C\, \underset{\sim}{\sigma}^{\rm dev} + F(\text{trace}\, \underset{\sim}{\sigma})\, \underset{\sim}{\mathbf{1}} \right) \tag{91}$$

according to the normality rule adopted here for simplicity.

In the case of tension in direction 2, the direction of plastic flow becomes

$$[P] = \frac{\text{signe}\, \sigma_2}{\sqrt{C+F}} \begin{bmatrix} F - \frac{C}{2} & 0 & 0 \\ 0 & C+F & 0 \\ 0 & 0 & F - \dfrac{C}{2} \end{bmatrix} \tag{92}$$

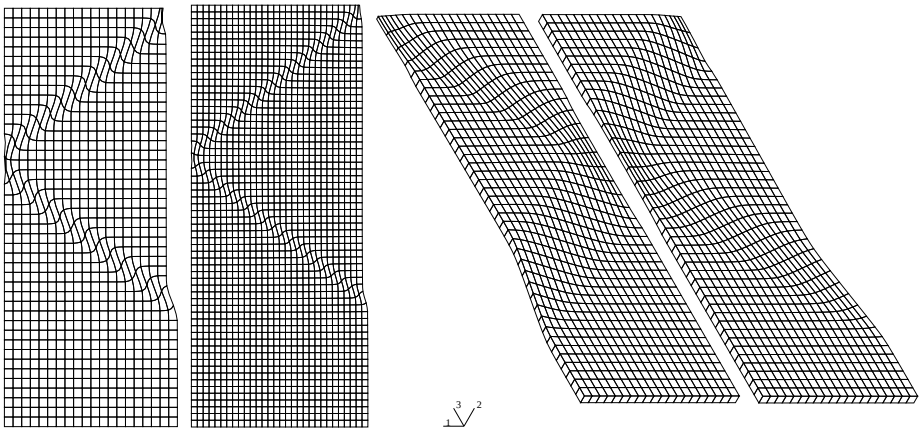

Figure XI.7: Simulation of strain localization in a von Mises elastoplastic material in tension in 2D and 3D case.

The bifurcation analysis under plane stress conditions was performed in section 1.2.4 in the general case trace $\underset{\sim}{\mathbf{P}} \neq 0$. It can therefore be applied to the elliptic potential. Under plane stress conditions, the orientation of the first possible localization is given by the equation (73) which reads here:

$$n_1^2 = \frac{2}{3C}\left(\frac{C}{2} - F\right) \tag{93}$$

The same orientation is obtained taking the result (62) of the three–dimensional analysis for $\nu = 0$.

If $F = C/2$, it can be seen that both $\vec{n}$ and $\vec{g}$ are along direction 2. This corresponds to an horizontal strain localization band with an opening mode. If $F = 0$, the von Mises criterion is retrieved and the orientation of the band at 54° is recovered. As result, the elliptic model makes it possible to simulate strain localization bands inclined at an angle ranging from 0 to 54°.

1.4 RATE-DEPENDENT CONSTITUTIVE BEHAVIOR

The well-posed character of the set of equations characterizing the evolution of damage fields is based on the ellipticity of the corresponding linear solid of comparison (tangent operator of the dissipative branch). In the context of rate-dependent constitutive behavior, the tangent operator is derived through the instantaneous response of the material, generally the elastic part of the behavior, thus always definite positive. Therefore, rate-dependent damage laws should not result in ill-posed problems. This explains why introducing viscous terms in damage laws has appeared as a convenient way to regularize the ill-posed problems of rate-independent laws, see Needleman (1988).

However, a linear perturbation analysis shows that, even though well-posed, that kind of problems becomes unstable beyond a given state (Fressengeas and Molinari, 1985; Anand et al., 1987; Dobovsek and Moran, 1996). The instability takes the form of a localization band. Moreover, Needleman (1988) illustrated by a 1D example that the localization is triggered by imperfections whose length scale introduces a size for

the localization band. Indeed, from a dimensional point of view, new viscous terms only introduce a characteristic time. Alone, it does not bring a characteristic length for the localization band, at least for quasi-static analysis.

Here, we would like to somewhat extend Needleman's example, so that no homogeneous solutions are allowed, even piecewise, while preserving the 1D character. For that purpose, we go back to the rod already studied but we now assume that its cross section area S is variable:

$$S(x) = S_0 \ \left(1 - \frac{x}{\lambda}\right)^{-1} \qquad 0 \leq x \leq L \quad \text{and} \quad L < \lambda$$

where L is the rod length and λ a characteristic length scale of the heterogeneity. This new length scale is involved in the equilibrium equation since it reads:

$$\frac{\partial}{\partial x}\left(S\,\sigma\right) = 0 \qquad \Rightarrow \quad \sigma(x,\ t) = \Sigma(t)\ \left(1 - \frac{x}{\lambda}\right) \tag{94}$$

Contrary to the homogeneous example, the stress field now depends not only on the time but also on the spatial position, with the special form given in (94) thanks to the equilibrium equation. The constitutive equation is a Duvaut-Lions viscous regularization (Duvaut and Lions, 1976) of the damage model (8)-(10), which in the 1D context reduces to:

$$\sigma = (1-d)\ E\,\varepsilon \tag{95}$$

$$\dot{d} = \frac{1}{k\,\tau}\left\langle \frac{1}{2} E\,\varepsilon^2 - w^y(d) \right\rangle \qquad \text{where} \quad \langle x \rangle = \frac{x + |x|}{2} \tag{96}$$

where the new material parameter τ has indeed the dimension of a time. Finally, the load is representative of a relaxation test, that is a displacement U is instantaneously prescribed at time $t = 0$ on one end of the rod, the other remaining clamped. It appears that the load does not bring any new characteristic time, so that the various fields solutions of the problem depend on the time only through the normalized time $\bar{t} = t/\tau$: this is the only influence of the characteristic time τ associated to viscosity.

At the initial time $t = 0$, the damage zone corresponds to the area where $\dot{d} > 0$. A straightforward calculation with $d = 0$ shows that there is damage inception in a band of width:

$$w_0 = 1 - \frac{2 - L/\lambda}{2U/L}\varepsilon^y \qquad \text{as soon as} \quad U \geq U^c = L\left(1 - \frac{L}{2\lambda}\right)\varepsilon^y$$

It proves that the initial band width w_0 depends not only on the heterogeneity length scale λ but more generally on the material parameters and on the load level U itself.

A closed-form solution does not seem available for the further evolution of the damage distribution and namely the band width $w(t)$. Therefore, the solution is dealt numerically. The results are presented in figure XI.8 for the following set of parameters (no units, thanks to the normalization of L, E and τ):

$$L = 1 \quad E = 1 \quad \tau = 1 \quad k = 5.6125\ 10^{-8} \quad \gamma = 0.25 \quad \lambda = 10 \quad U/U^c = 1.02$$

The following facts can be observed:

- With increasing time, the damage level at the smallest cross-section ($x = 0$) increases while the band width (within which damage goes on evolving) decreases, thus leading to an increasing damage gradient.

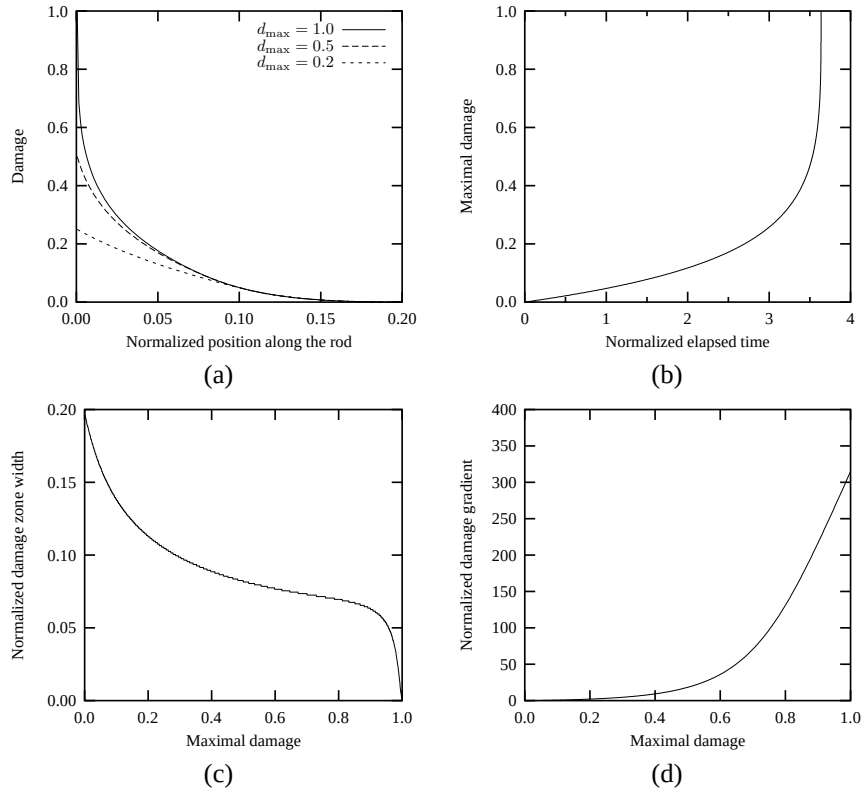

Figure XI.8: (a) Damage spatial evolution; (b) Maximal damage evolution; (c) Evolution of the width of the damaged zone; (d) Damage gradient evolution.

- There exists a critical time beyond which the previous observations are dramatically strengthened. Namely, the damage rate highly increases while the localization width goes to zero, resulting in a very large damage gradient.

From a purely numerical ground, the fact that the band width tends to zero when damage increases may raise again the issue of spurious mesh-dependency. This is confirmed by the numerical simulation of the perforated plate with a material obeying the Duvaut-Lions viscous regularization of the rate-independent evolution law (9)-(10). A given instantaneous displacement is prescribed on both sides of the plate. On figure XI.9, the localization of damage in a band of width equal to the size of a single element is apparent beyond some damage level. This is independent of the viscosity parameter value because it only induces a change in the time scale, as in the 1D example. In addition, the numerical treatment of such problems is somewhat difficult regarding the time discretization scheme. Indeed, on the one hand, Cherukuri and Shawki (1995) have shown that the stability of explicit schemes is ensured only with time steps far smaller that those required by the usual stability conditions (based on a linear analysis). On the other hand, Simo (1988) has shown that implicit schemes become only conditionally stable and therefore also require a close attention to the time–stepping.

In our opinion, these observations put severe restrictions on the use of viscous

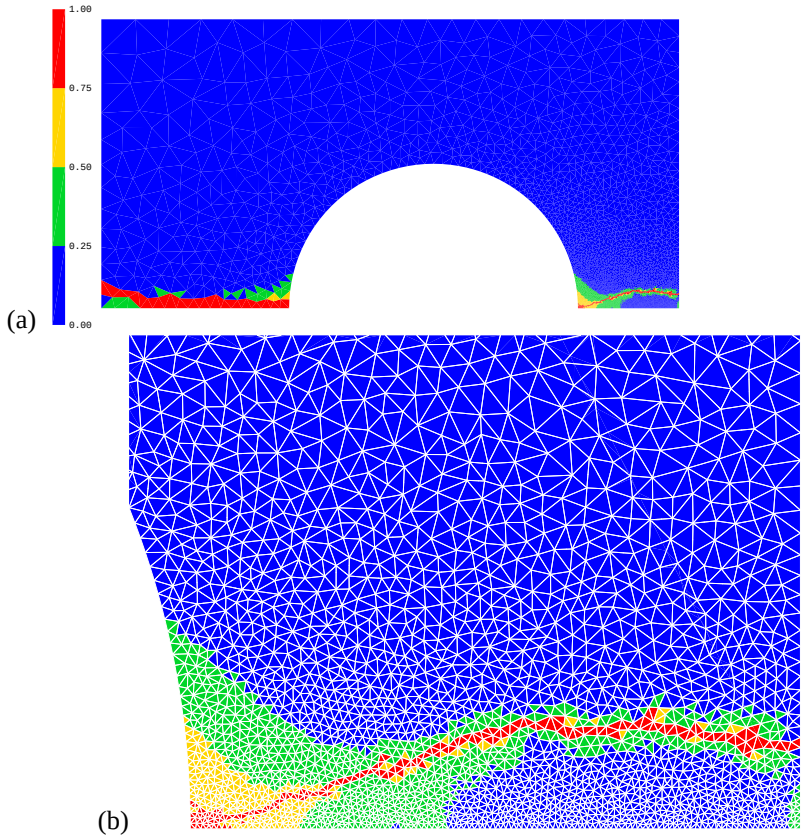

Figure XI.9: Damage distribution with viscosity for a relaxation test: (a) whole specimen, (b) close–up at the right side of the hole.

regularization as a way to control damage localization. However, the essential fact that demonstrates that viscous regularization alone is not sufficient concerns the high increase of the spatial damage gradient, observed in both examples and in the literature, even for dynamic simulations (Needleman, 1988). For physical reasons that will be detailed in the next section, usual local constitutive relations, time-dependent as well as time-independent, fail at characterizing the material behavior in the presence of large gradients of the mechanical fields. This conclusion is based on a specific viscous law and other ones may lead to more favourable results Ladevèze (2000).

1.5 STRAIN LOCALIZATION INDICATORS IN NUMERICAL SIMULATIONS AT FINITE STRAINS

Rice's condition for localization can be used to derive indicators to detect the onset of possible numerical localization in finite element simulations (Billardon and Doghri, 1989; Doghri and Billardon, 1995; Besson et al., 2001b, 2003). Following Rice and Rudnicki (1980) and Mear and Hutchinson (1985) in the case of finite strains, the localization criterion is expressed as:

$$\det \underset{\sim}{\mathbf{A}}(\vec{n}) = 0 \text{ with } \underset{\sim}{\mathbf{A}}(\vec{n}) = \vec{n}.\underset{\approx}{\mathbf{D}}.\vec{n} + \underset{\sim}{\mathbf{R}} \tag{97}$$

where the tensor $\underset{\sim}{\mathbf{R}}$ is given by

$$2\,\underset{\sim}{\mathbf{R}} = -\vec{n}\otimes(\vec{n}.\underset{\sim}{\sigma}) + (\vec{n}.\underset{\sim}{\sigma})\otimes\vec{n} + (\vec{n}.\underset{\sim}{\sigma}.\vec{n})\,\underset{\sim}{\mathbf{1}} - \underset{\sim}{\sigma} \tag{98}$$

when the objective stress rate is taken as the Jauman rate.

A localization indicator can then be defined as:

$$I_l = \min_{\vec{n},\,||\vec{n}||=1} \det \underset{\sim}{\mathbf{A}}(\vec{n}) \tag{99}$$

At a given material point, localization can occur as soon as $I_l = 0$. When performing a structural finite element calculation, the condition $I_l = 0$ taken over the whole structure can be used as a criterion for failure initiation (Billardon and Doghri, 1989). Beyond this point the problem is likely to be ill-posed, and the condition can also be used to stop the calculations.

An example of application is given in figure XI.10 in the case of the Gurson model. The indicator in normalized using the value of $\det \vec{n}.\underset{\approx}{\mathbf{D}}.\vec{n}$, D_e, when $\underset{\sim}{\mathbf{D}}$ is equal to the elasticity tensor. One gets:

$$D_e = \det \vec{n}.\underset{\approx}{\mathbf{E}}.\vec{n} = \frac{1}{4}\frac{(1-\nu)E^3}{(1-2\nu)(1+\nu)^3} \qquad \forall \vec{n} \tag{100}$$

for isotropic elasticity. The localization angle can also be determined. It corresponds to the orientation of the vector, $\vec{n}_0$, minimizing $\det \underset{\sim}{\mathbf{A}}$. The direction of the velocity jump across the localization band, $\vec{g}$, is computed as the eigenvector corresponding to the lower eigenvalue of $\underset{\sim}{\mathbf{A}}(\vec{n}_0)$. One notices that in the case of figure XI.10, the localization angle is slightly larger than $45°$. This is due to the plastic dilatancy of the constitutive equation.

An example of application of the localization indicator is given in the following concerning the simulation of cup–cone fracture of tensile bars (Tvergaard and Needleman, 1984; Besson et al., 2001b). In absence of regularization, the mesh is designed so that cup-cone fracture numerically occurs. An numerical investigation, has shown that it is desirable to have approximatively square elements at the onset of localization. The calculation shown on figure XI.11 was performed using quadratic elements (8 nodes) with reduced integration (4 Gauss points).

The evolution of damage f and of the localization indicator I_l is detailed in figure XI.11 during cup–cone formation. After the maximum load has been reached, progressive necking is observed and the specimen can be divided into two regions: elastic unloading and plastic loading ((1) in figure XI.11). Damage is concentrated at the center of the necked region so that the localization indicator becomes negative (2). This also corresponds to the sharp slope change on the normalized load F/S_0— diameter reduction $\Delta d/d_0$ curve (F: force, S_0 initial cross section, Δd: diameter variation, d_0 initial diameter). The diameter reduction is monitored in the initial symmetry plane. The highly damaged zone grows and leaves, behind its tips, an elastically unloaded zone which correspond to the flat portion of the cup–cone (3) and forms a penny–shaped crack. Ahead of this zone, two "wings" where the localization criterion is met, develop and become larger as the central crack grows (3)—(5). Crack deflection starts with a relatively small angle. Deflection seems to be possible when the localization wings extend over 2 and more elements. At step (5) the wings have grown sufficiently so that the cup–cone develops (6)(7). At some point, the diameter does not

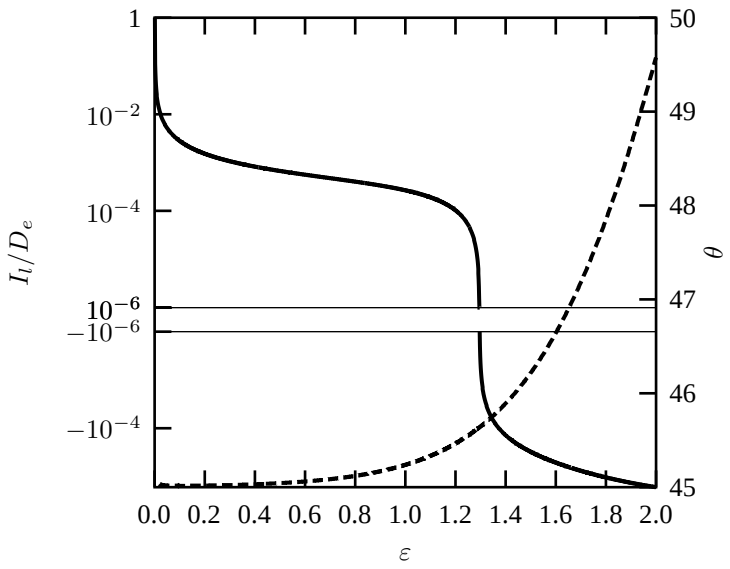

Figure XI.10: Minimum value of the localization indicator (full line) and localization angle (dashed line), θ, as a function of the deformation under plane strain condition (Gurson model).

vary any more. This occurs when the point of measure leaves the active plastic zone which is ahead of the highly damaged band.

At the center of the specimen where localization starts, the predicted localization angle is $\theta = \pm 60^\circ$ whereas the observed on is equal to 90°. Note that the experimental fracture surface remains flat as in the calculations. This result is likely due the the finite size of the localized band whereas Rice's analyze is valid for an infinite medium. Once the crack has left the center of the specimen, the agreement between the predicted angle and the simulated one becomes better Besson et al. (2001b): it is possibly related to the increase of the localization "wings".

1.6 THE NEED FOR CHARACTERISTIC LENGTHS

It has been seen that the mathematical description of the damage problem becomes ill-posed, at least in the context of rate-independent materials, so that the predicted width of the localization bands is zero. Nevertheless, the localization phenomenon as a concentration of the strain and the damage in narrow bands is indeed in agreement with physical observations. It implies that the length scale of the macroscopic mechanical fields becomes of the same magnitude as the microstructural length scale, thus precluding the main homogenization hypothesis of scale separation: classical homogenization is no more valid to derive the local constitutive laws. We think this is the key point that explains why usual damage constitutive relations fail to predict damage propagation within a structure, since they rely implicitly or not on this scale separation assumption.

It should be noticed that the inadequacy of usual constitutive laws is not specific of Damage Mechanics. There are other domains where the scale introduced through the

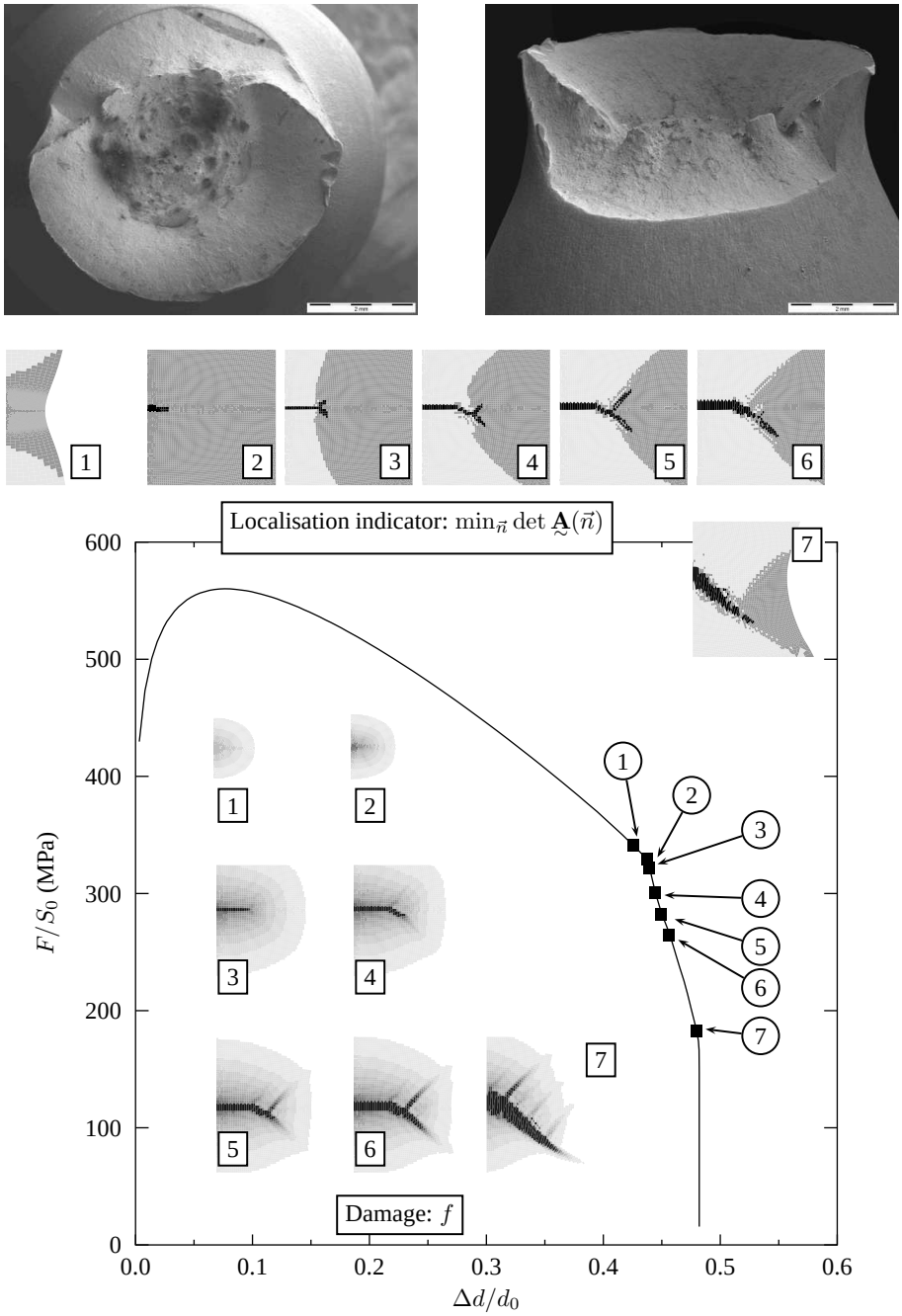

Figure XI.11: Load vs. diameter reduction curve and cup–cone formation for a round bar. Contour maps indicate damage (white: $f = 0$, black: $f > 0.1$) and the localization indicator (white: elastic unloading, gray: plastic loading, black plastic loading and negative indicator). Photographs give an example of cup–cone fracture in a HSLA steel (Rivalin, 1998).

loading conditions is close to the microstructure scale. In that cases too, there is a need for new types of constitutive equations to get quantitative predictions in agreement with the experiments, even though the problem remains well-posed, on the contrary of damage ones. Thus, many observed phenomena are known in the literature whereby the smaller the size, the stronger the response. For instance, indentation hardness of metals and ceramics increases as the size of the indenter is decreased (Stelmashenko et al., 1993).

Several authors have proposed to enrich the homogenization schemes to include this length scale interaction. When the interaction is given a priori, (Drugan and Willis, 1996) succeeded in deriving a homogenized nonlocal constitutive law. However, the task becomes harder when the interaction results from the evolution of the macroscopic fields themselves, as for localization. Then, only rough approximations have been obtained so far. Thus, in the context of hyperelasticity, Bardenhagen and Triantafyllidis (1994) introduced strain gradient terms into the energy based on the analysis of a periodic lattice. For ductile damage, Gologanu et al. (1997) enhanced Gurson's model by taking into account gradient effects on the boundary of the elementary representative volume ; it also resulted in the introduction of strain gradient terms. Andrieux et al. (1996) proposed a homogenization scheme to get some guidelines for the introduction of the gradient of internal variables into the energy, based on the replacement of Taylor's scheme by a first order variation of the macroscopic internal variable field inside a patch of elementary representative cells. Other authors preferred to introduce scale effects on the basis of phenomenological propositions, mainly in the context of metal plasticity where the mechanism of dislocation interaction is well studied, see for instance (Gao et al., 1999; Fleck and Hutchinson, 1993; Forest et al., 2000).

Whatever their bases, all these approaches result in the introduction of some characteristic lengths of the microstructure in the macroscopic equations. These new length scales will in turn control the localization of the macroscopic fields, allowing to retrieve a well-posed problem the solution of which is no more spuriously set by the spatial discretization. In particular, the width of the localization bands does not tend to zero, so that a finite non vanishing amount of energy is dissipated by the damage mechanism.

2 REGULARIZATION METHODS

Any enhancement of the constitutive or even continuum model that is able to remove the spurious mesh–dependency observed in the simulation of strain localization phenomena is called a regularization method. It introduces generally additional intrinsic length scales into the modeling that lead to finite width strain localization bands. The pioneering work of the dutch school (de Borst, 1991, 1993; de Borst et al., 1993) is based on a reappraisal of the mechanics of generalized continua developed in the 1960s (Kröner, E., 1967; Forest et al., 2001). Generalized continua can be classified into 3 main groups. Higher order continua are endowed with additional degrees of freedom in addition to the usual displacement field (Cosserat and micromorphic theories, according to Eringen (1976)). Higher grade continua introduce higher space derivatives of the displacement field than the usual deformation gradient (second gradient theory according to Mindlin and Eshel (1968)). This group of theories also includes the gradient of internal variable approach that lets the gradient of some selected internal variable play a role in the balance and constitutive relations (Aifantis, 1987). The last class contains fully nonlocal media for which integral relations relate stress and

strain evolutions (Eringen, 1976; Pijaudier-Cabot and Bazant, 1987). Examples of such enhancements are given below, that show the presence of an intrinsic length scale in the equations and its effect on strain localization phenomena.

2.1 A TOOL TO EXPLORE NONLOCALITY

As confirmed by the huge number of publications dedicated to the subject over the past thirty years, there are many ways to introduce characteristic lengths into constitutive models, resulting in so-called "nonlocal models". Because of the diversity, there is a need for a general framework to encompass several of these nonlocal models, aiming at a unified formulation to better understand their differences and explore their properties. Unfortunately, a unified framework implies some abstraction and the reader interested only in a given nonlocal model may skip this part.

As soon as nonlocality is introduced, we think that the material point is no more the right scale to express the constitutive laws namely because of the constitutive interactions between distinct material points: the scale of the structure should be preferred. However, this cannot be achieved in a systematic way for any type of constitutive laws. Therefore, we restrict our attention to the class of rate-independent generalized standard materials. Moreover, for the sake of simplicity, no thermal coupling will be considered and the material is assumed isothermal.

2.1.1 Generalized standard materials

The concept of generalized standard materials has been introduced as a special class of constitutive laws initially by Halphen and Nguyen (1975) in the context of plasticity. It has then been extended to various dissipative phenomena, see Nguyen (1993), to provide a general expression for the evolution laws of internal variables, in intimate relation with the notion of normal and associated flow rules in plasticity, that is the principle of maximal dissipation. On a thermodynamical ground, its energetic bases ensure that the second principle of thermodynamics, under the form of the Clausius–Duhem inequality in mechanics, is automatically fulfilled, while on a mathematical ground, it relies on convex analysis, see Moreau (1970) for the relation with Mechanics and Ekeland and Temam (1974) for essential mathematical results. Finally, the reader is also referred to Lemaitre and Chaboche (1994) for a pedagogical presentation.

In this framework, the local material state is described by means of the strain tensor $\underset{\sim}{\varepsilon}$ and a set of independent internal variables a. The definitions of the stress tensor $\underset{\sim}{\sigma}$ and the driving forces A associated to a are given by the state equations which derive from the free Helmholtz energy Φ:

$$\underset{\sim}{\sigma}(\vec{x}) = \frac{\partial \Phi}{\partial \underset{\sim}{\varepsilon}} \left(\underset{\sim}{\varepsilon}(\vec{x}),\ a(\vec{x}) \right) \qquad A(\vec{x}) = -\frac{\partial \Phi}{\partial \alpha} \left(\underset{\sim}{\varepsilon}(\vec{x}),\ a(\vec{x}) \right) \tag{101}$$

Thanks to these definitions, the mechanical dissipation (the only dissipation source) is equal to:

$$D(\vec{x}) = \underset{\sim}{\sigma}(\vec{x}) : \dot{\underset{\sim}{\varepsilon}}(\vec{x}) - \dot{\Phi}(\vec{x}) = A(\vec{x})\, \dot{a}(\vec{x}) \tag{102}$$

The driving forces govern the rate of the internal variables $\dot{a}$ through a flow rule and a consistency condition which rely on a convex threshold function $g(A)$:

$$\dot{a}(\vec{x}) = \lambda(\vec{x})\, \frac{\partial g}{\partial A}\left(A(\vec{x})\right) \tag{103}$$

$$g\left(A(\vec{x})\right) \leq 0 \qquad \lambda(\vec{x}) \geq 0 \qquad \lambda(\vec{x})\; g\left(A(\vec{x})\right) = 0 \tag{104}$$

λ is the plastic multiplier, in reference to plastic behavior. The set of driving forces that fulfill the inequality $(104)_a$ is the domain of reversibility K of the constitutive behavior which, by assumption, should contain $A = 0$:

$$K = \{A\ ;\ \ g(A) \leq 0\}$$

An explicit reference to the material point through its coordinates $\vec{x}$ is made in the previous equations to allow a clear distinction between a field and its value at a given point, for instance the strain field $\underset{\sim}{\varepsilon}$ and the local strain tensor $\underset{\sim}{\varepsilon}(\vec{x})$.

As an illustration, consider the damage model described through equations (8) to (10). At first sight, it does not belong to the framework of generalized standard materials because its threshold function g depends explicitly on the strain tensor, on the contrary of (103)–(104). However, we consider the following free energy, which depends on the strain tensor and the damage variable:

$$\Phi\left(\underset{\sim}{\varepsilon}, d\right) = \frac{1}{2}\,(1-d)\ \underset{\sim}{\varepsilon} : \underset{\approx}{\mathbf{E}} : \underset{\sim}{\varepsilon} + k\ \frac{d\,(d-1)}{1+\gamma-d}$$

The stress–strain relation (8) is retrieved at once, while the driving force associated to damage is defined by:

$$A = -\ \frac{\partial \Phi}{\partial d}\left(\underset{\sim}{\varepsilon}, d\right) = \frac{1}{2}\ \underset{\sim}{\varepsilon} : \underset{\approx}{\mathbf{E}} : \underset{\sim}{\varepsilon} + k - w^y(d)$$

Then, it can be noticed that the evolution equations (9)-(10) are equivalent to (103)-(104) when choosing the following threshold function g that depends only on the driving force A:

$$g\left(A\right) = A - k$$

2.1.2 Introduction of a dissipation potential

The evolution equation (103)-(104) can be expressed in a more compact way that allows a relation with the expression of the dissipation. For that purpose, the dissipation potential Ψ is introduced through a Legendre transform of the (indicator of the) threshold function f:

$$\Psi\left(\dot{a}(\vec{x})\right) \underset{def.}{=} \underset{A \in K}{\mathrm{Sup}}\ A(\vec{x})\,\dot{a}(\vec{x}) \tag{105}$$

Generally, the dissipation potential is not a regular function. It may include indicator functions resulting in constraints for the internal variable rate ($e.g.$ damage only increases, plastic strain remains isochoric, *etc*.). Besides, in the context of rate-independent material, it is positive homogeneous of degree one (like the norm function, for instance) and therefore, it is often not differentiable for $\dot{a} = 0$.

To overcome the lack of regularity, we rely on the notion of subgradient which extends usual derivatives for convex non differentiable functions. In the present case, the subgradient of Ψ for a given rate $\dot{a}(\vec{x})$ is defined as the set of driving forces which realize the maximum (105):

$$\partial\Psi\left(\dot{a}(\vec{x})\right) = \left\{A \in K\ ;\ \ \forall\ \hat{A} \in K\ \ A\,\dot{a}(\vec{x}) \geq \hat{A}\,\dot{a}(\vec{x})\right\} \tag{106}$$

A characterization of the maximum (105) is actually provided by Euler equation (103) and Kuhn and Tucker condition (104). It means that the evolution equations (103)-(104) are equivalent to the following more compact statement:

$$A(\vec{x}) \in \partial\Psi\left(\dot{a}(\vec{x})\right) \tag{107}$$

Regarding the dissipation, it appears that if the internal variable rate obeys the evolution equation (107), the dissipation is maximized, according to (106): this is the principle of maximal dissipation. As $A = 0$ belongs to the domain of reversibility K, it immediately implies that the dissipation is positive, that is the Clausius – Duhem inequality is automatically fulfilled by generalized standard materials.

To illustrate the notion, the dissipation potential corresponding to the damage model is exhibited:

$$\Psi\left(\dot{\alpha}\right) = \underset{A \leq k}{\text{Sup}}\; A \cdot \dot{\alpha} = \begin{cases} +\infty & \text{if } \dot{\alpha} < 0 \\ k\,\dot{\alpha} & \text{if } \dot{\alpha} \geq 0 \end{cases} \quad = k\,\dot{\alpha} + I_{\mathbb{R}^+}\left(\dot{\alpha}\right) \tag{108}$$

where I_C denotes the indicator function of a closed convex set C: it is zero valued inside C and equal to $+\infty$ outside C.

2.1.3 Extension to the scale of the structure

In the context of generalized standard materials, the constitutive behavior is totally defined using two energetic potentials, the free energy and the dissipation potential. This is an appropriate starting point to extend the constitutive laws from the material point scale to the structural scale. Following Lorentz and Andrieux (1999), a global free energy and a global dissipation potential are defined as the sum of the local ones over the whole structure, where Ω denotes the body domain:

$$F\left(\underset{\sim}{\varepsilon},\ a\right) \underset{def.}{=} \int_{\Omega} \Phi\left(\underset{\sim}{\varepsilon}(\vec{x}),\ a(\vec{x})\right)\, dx \tag{109}$$

$$D\left(\dot{a}\right) \underset{def.}{=} \int_{\Omega} \Psi\left(\dot{a}(\vec{x})\right)\, dx \tag{110}$$

The constitutive law can be expressed at the global scale formally in a similar way as at the material point scale, that is:

$$\underset{\sim}{\sigma} = \frac{\partial F}{\partial \underset{\sim}{\varepsilon}}\left(\underset{\sim}{\varepsilon}, a\right) \qquad A = -\,\frac{\partial F}{\partial a}\left(\underset{\sim}{\varepsilon}, a\right) \tag{111}$$

$$A \in \partial D\left(\dot{a}\right) \tag{112}$$

Now the state variables are the strain and internal variable fields while the driving forces are linear forms operating on these fields. It is yet essential to note that the global law (111)-(112) is totally equivalent to the local one (101)-(104) expressed at every point $\vec{x}$ of the structure. We believe this is the appropriate level to introduce nonlocality into the constitutive model.

2.1.4 Time integration: a minimum principle

It is still possible to go one step further by discretising the global constitutive equations (111)-(112) with respect to time. The objective is to obtain a characterisation of the internal variable evolution as a minimization problem. Let us focus on a single time-increment $[t_n,\ t_{n+1}]$, where q_n and q_{n+1} denote respectively the value of a quantity q at the beginning and the end of the increment. $\Delta q = q_{n+1} - q_n$ denotes its variation during the increment. The use of Euler backward scheme leads to the following discretized constitutive equations, corresponding respectively to the state equations (111) and the evolution equation (112):

$$\underset{\sim}{\sigma}_{n+1} = \frac{\partial F}{\partial \underset{\sim}{\varepsilon}}\left(\underset{\sim}{\varepsilon}_{n+1}, a_{n+1}\right) \qquad A_{n+1} = -\frac{\partial F}{\partial a}\left(\underset{\sim}{\varepsilon}_{n+1}, a_{n+1}\right) \tag{113}$$

$$a_{n+1} \in \partial D\left(\frac{\Delta a}{\Delta t}\right) \tag{114}$$

A combination of both discretized equations to eliminate the driving forces results in:

$$-\frac{\partial F}{\partial a}\left(\varepsilon_{n+1}, a_{n+1}\right) \in \partial D\left(\frac{\Delta a}{\Delta t}\right) \tag{115}$$

This is the characterization of a minimum. Namely, the internal variable field a_{n+1} at the end of the time-step realizes the following minimum:

$$\begin{aligned} a_{n+1} \quad = \quad & \underset{a}{\arg\min}\ E\left(\underset{\sim}{\varepsilon}_{n+1}, a\right) \\ & \text{where} \quad E\left(\underset{\sim}{\varepsilon}, a\right) = F\left(\underset{\sim}{\varepsilon}, a\right) + \Delta t\, D\left(\frac{a - a_n}{\Delta t}\right) \end{aligned} \tag{116}$$

In the case of rate-independent materials, the dissipation potential is positive homogeneous of degree one, which implies that the time-step length Δt disappears from the expression of E, resulting in:

$$E\left(\underset{\sim}{\varepsilon}, a\right) = F\left(\underset{\sim}{\varepsilon}, a\right) + D\left(a - a_n\right) \tag{117}$$

Actually, the minimum principle would be preserved if the dependence of the strain field on the displacement field $\vec{u}$ was explicitly expressed and if the virtual external work $W_{ext}(\vec{u})$ was subtracted from E. It leads to the following incremental potential energy, where the attribute "incremental" is set to remind that the function also depends on the values of the internal variables a_n at the beginning of the time-increment:

$$E_{pot}\left(\vec{u}, a\right) = F\left(\underset{\sim}{\varepsilon}(\vec{u}), a\right) + D\left(a - a_n\right) - W_{ext}(\vec{u}) \tag{118}$$

Thanks to the expression (113) of the stress field, the minimization with respect to the displacement field then results in the variational formulation of the equilibrium equation, the principle of virtual power:
$\forall\ \delta\vec{u} \in KA^0$

$$\left\langle \frac{\partial E_{pot}}{\partial \vec{u}}(\vec{u}_{n+1}, a_{n+1}) \;\middle|\; \delta\vec{u} \right\rangle = \int_{\Omega} \underset{\sim}{\sigma}_{n+1}(\vec{x}) : \underset{\sim}{\varepsilon}\left(\delta\vec{u}(\vec{x})\right)\ dx - \delta W_{ext} = 0 \tag{119}$$

where *KA* denotes the set of kinematically admissible displacements, KA^0 the corresponding vector space (the set of admissible virtual velocities) and the brackets $\langle \cdot \mid \cdot \rangle$ denote the duality product.

In conclusion, a variational formulation of the constitutive relation at the scale of the structure has been proposed. After time-discretization, it can be expressed as a minimum principle. Moreover, the equilibrium equations may also be expressed as a minimum principle. Thus, the solution $(\vec{u}_{n+1}, a_{n+1})$ of the problem at the end of the time-step realizes the following minimizations:

$$\begin{aligned} \vec{u}_{n+1} &= \underset{\vec{u} \in KA}{\arg\min}\ E_{pot}\left(\vec{u}, a_{n+1}\right) \\ a_{n+1} &= \underset{a}{\arg\min}\ E_{pot}\left(\vec{u}_{n+1}, a\right) \end{aligned} \tag{120}$$

The simultaneous minimization with respect to both variables is not equivalent to (120) as soon as the potential energy is not convex with respect to the couple $(\vec{u}, a)$. It is more restrictive and may be set as a criterion for the stability of the solution, see Francfort and Marigo (1993).

2.2 SPATIAL REGULARIZATION OF THE MECHANICAL VARIABLES

One of the first attempts to introduce some characteristic lengths into a constitutive law consists in substituting a smoothed variable or a smoothed driving force for its local counterpart into the state equations, the flow rule or the consistency condition. The purpose is evidently to smooth up the abrupt spatial variations of the mechanical fields observed in localization bands. This pragmatic way of introducing some regularization has been used by several authors in the past and is still intensively applied in the context of brittle damage, see for instance (Bazant and Pijaudier-Cabot, 1988; Peerlings et al., 1996; Comi, 2001; Pijaudier-Cabot and Bazant, 1987; Pijaudier-Cabot and Huerta, 1991; Comi and Perego, 2001) for the introduction of a nonlocal damage variable within the evolution law. Yet, it can be noticed that its application in the context of plasticity, and in particular ductile plasticity, is more seldom (Leblond et al., 1994; Tvergaard and Needleman, 1995; Baaser and Tvergaard, 2003).

2.2.1 Regularization operators

In the present approach, the first step is the choice of a regularizing operator **R**, acting on the strain field, the internal variable field or the driving forces. Consider for instance the internal variable field a. This operator produces the smoothed internal variable field, say $\bar{a}$, which is an element of a new space of functions V_R, desirably " smoother " than the functions of the space of the original internal variable fields V:

$$\begin{aligned} \mathbf{R} \quad : \quad V \quad &\rightarrow \quad V_R \subset V \\ a \quad &\mapsto \quad \bar{a} = Ra \end{aligned}$$

The definition of the operator **R** may rely on an integral as well as a differential characterization, see for instance the frequently used Gaussian convolution operator **M**, introduced by Eringen (1972) in the context of nonlocal elasticity, or the gradient penalty operator **P**, Peerlings et al. (1996), which both involve a characteristic length L_c:

$$\left(\mathbf{M}\, a\right)(x) = \bar{a}(x) = \int_{\Omega} \omega\left(x,\ y\right)\ a\left(y\right)\ dy$$

$$\text{with} \quad \begin{cases} \omega\,(x,\ y) = \dfrac{1}{V_r(x)} e^{-\dfrac{\|x-y\|^2}{2\,L_c^2}} \\ V_r(x) = \displaystyle\int_\Omega e^{-\dfrac{\|x-y\|^2}{2\,L_c^2}}\, dy \end{cases} \tag{121}$$

$$\mathbf{P}\,a = \bar{a} \quad \text{solution of} \quad \begin{cases} \bar{a} - L_c^2\,\Delta\bar{a} = a & \text{in } \Omega \\ \nabla\bar{a}\cdot\mathbf{n} = 0 & \text{on } \partial\Omega \end{cases} \tag{122}$$

Two natural demands arise on regularizing operators: they must leave unchanged the constant fields and be injective. The latter demand is based on the physical consideration that the "true" state variable which is used for the description of the local thermodynamic state of the material is the non smoothed one, so that it must be determined uniquely from the smoothed one. Remark also that the linearity of the operator $\mathbf{R}$ is a matter of convenience which ensures in particular that the regularization involved in the rate constitutive equations is the same (differentiation of a linear operator leads to itself).

2.2.2 An attempt toward a classification

The second step of the present nonlocal approach consists in substituting the smoothed state variable or driving force for its local counterpart into part of or all the equations of the problem. Obviously, there is a wide range of combinations, depending on which variables are replaced by their smoothed counterparts and where they are. The situation is somewhat confusing because all the resulting models do not possess the same properties, especially regarding localization control.

Lorentz and Andrieux (2003) have tried to make a classification of the formulations, thus allowing a study of their generic properties, independently of the local constitutive laws under consideration. Three classes of properties have been distinguished:

- Effect on a well-posed problem: when applying a regularization technique to a local problem which is an initially well-posed, does it result in a still well-posed nonlocal problem ?
- Thermodynamics: does the nonlocal model fulfills the second principle of Thermodynamics (Clausius – Duhem inequality), as soon as the local one does ?
- Effective regularization: does the nonlocal model indeed select a minimal (non zero) width for the localization bands ?

The analysis relies on the interpretation of the equations of the problem as a minimization principle (120). Therefore, it is restricted to isothermal rate-independent materials whose local constitutive law belongs to the framework of generalized standard materials. Moreover, for the sake of simplicity in the presentation, the explicit dependence of the strain field to the displacement field is omitted, and so is the external virtual work. On this basis, only the strain field or the internal variable field may be smoothed by a regularization operator. The five possible combinations are gathered in table XI.2.

The conclusions of the analysis are the following:

- Coupled regularization. A smoothed variable (strain or internal variable) is introduced in both minima (117), characterizing respectively the equilibrium

and the constitutive relation. In that case, the regularization operator has to be coercive[2] to preserve solutions to initially well-posed problems. This is not achieved by the operators (121) and (122). Moreover, when using a coercive operator, the problem is no more regularized: initially ill-posed problems remain ill-posed.

- Split regularization. Smoothed internal variables are introduced into the free energy. It corresponds to a large class of nonlocal formulation where the driving forces are regularized. Again, a coercive operator is required to preserve the well-posed character of initially well-posed problem and, in that case too, no regularization is brought into the problem.

- Uncoupled regularization. A smoothed strain is introduced in the global constitutive equation, minimum (120), or smoothed internal variables are introduced in the equilibrium equation, minimum (120). In that case, the symmetry of the problem is lost, since a different potential is used in the equilibrium and the constitutive law. In particular, the second principle of Thermodynamics is no more automatically fulfilled. However, effective regularization is indeed brought into the problem: the width of localization band may be controlled.

In conclusion, except for very special nonlocal models which escape the general framework of the analysis, effective regularization and preservation of the grounding energetic basis cannot be gained together. This is related to the fact that such a kind of regularization is more pragmatic than based on physical derivations. Regarding this aspect, our preference goes to models with higher order gradients, as will be presented in the next parts. Nevertheless, the regularization approach has the merit of removing spurious mesh-dependency from the computations, as illustrated below.

2.2.3 Numerical application

To illustrate the potencies of introducing nonlocality through the regularization of some mechanical fields, we turn again our attention to the perforated plate already used as a benchmark to explore the properties of local models and viscous regularization, see figure XI.2. The loading and the constitutive behavior are still a stretching prescribed displacement and the damage law presented in section 1.1.2 with the material parameters given in table XI.1.

Relying on the conclusions of the previous section, we choose to adopt an uncoupled strain regularization. It means that a smoothed strain is used to compute the internal variable while the stress - strain relation relies on the local strain only. The corresponding constitutive equations read:

$$\underset{\sim}{\sigma} = (1-d)\ \underset{\approx}{\mathbf{E}} : \varepsilon \tag{123}$$

$$\bar{\underset{\sim}{\varepsilon}} = \mathbf{R}\, \underset{\sim}{\varepsilon} \tag{124}$$

$$g\left(\bar{\underset{\sim}{\varepsilon}},\ d\right) \leq 0 \qquad \dot{d} \geq 0 \qquad \dot{d}\, g\left(\bar{\underset{\sim}{\varepsilon}},\ d\right) = 0 \tag{125}$$

where g is still the threshold function defined in (9). The regularization operator (122) is preferred to (121) for the regularization step (124), with characteristic length $L_c = 15$ mm. Indeed, with (122), a new nodal unknown for the spatial discretization

[2] A function $f : E \to \mathbb{R}$ is coercive if $f(x) \to +\infty$ when $||x|| \to \infty$.

strain regularization	Internal variable regularization
$(\varepsilon_{n+1},\ a_{n+1}) = \underset{\varepsilon,\,a}{\arg\min}\ E(\mathbf{R}\,\varepsilon,\ a)$ $\Downarrow$ $\left\{\begin{array}{l}\varepsilon_{n+1} = \underset{\varepsilon}{\arg\min}\ E(\mathbf{R}\,\varepsilon,\ a_{n+1})\\ a_{n+1} = \underset{a}{\arg\min}\ E(\mathbf{R}\,\varepsilon_{n+1},\ a)\end{array}\right.$	$(\varepsilon_{n+1},\ a_{n+1}) = \underset{\varepsilon,\,a}{\arg\min}\ E(\varepsilon,\ \mathbf{R}\,a)$ $\Downarrow$ $\left\{\begin{array}{l}\varepsilon_{n+1} = \underset{\varepsilon}{\arg\min}\ E(\varepsilon,\ \mathbf{R}\,a_{n+1})\\ a_{n+1} = \underset{a}{\arg\min}\ E(\varepsilon_{n+1},\ \mathbf{R}\,a)\end{array}\right.$
	$(\varepsilon_{n+1},\ a_{n+1}) = \underset{\varepsilon,\,a}{\arg\min}\ F(\varepsilon,\ \mathbf{R}\,a) + D(a - a_n)$ $\Downarrow$ $\left\{\begin{array}{l}\varepsilon_{n+1} = \underset{\varepsilon}{\arg\min}\ F(\varepsilon,\ \mathbf{R}\,a_{n+1}) + D(a_{n+1} - a_n)\\ a_{n+1} = \underset{a}{\arg\min}\ F(\varepsilon_{n+1},\ \mathbf{R}\,a) + D(a - a_n)\end{array}\right.$
$\left\{\begin{array}{l}\varepsilon_{n+1} = \underset{\varepsilon}{\arg\min}\ E(\varepsilon,\ a_{n+1})\\ a_{n+1} = \underset{a}{\arg\min}\ E(\mathbf{R}\,\varepsilon_{n+1},\ a)\end{array}\right.$	$\left\{\begin{array}{l}\varepsilon_{n+1} = \underset{\varepsilon}{\arg\min}\ E(\varepsilon,\ \mathbf{R}\,a_{n+1})\\ a_{n+1} = \underset{a}{\arg\min}\ E(\varepsilon_{n+1},\ a)\end{array}\right.$

Table XI.2: Different types of energy regularizations. The three rows correspond respectively to coupled, split and uncoupled regularizations.

of the smoothed strain field and a new corresponding balance equation (122) are introduced. This preserves the usual architecture of finite element software whereas (121) results in a coupling between Gauss points of distinct finite elements, which is far more unusual. Details on the finite element implementation are given in Godard (2001). We just mention that the contributions of Gauss points where damage has reached its ultimate value $d = 1$ have to be removed from the equation (124) to avoid the spurious enlargement of the damaged zone observed in Peerlings (1999). This artificial procedure is a direct consequence of the already mentioned pragmatism of the approach.

The numerical results are presented in figure XI.12 in terms of the damage distribution a little bit before the ultimate fracture of the specimen: one of the ligaments of the plate is totally broken while the second is crossed by a propagating damaged zone. It can be observed that the localization band width spreads over several finite elements and is normal to the tensile direction, which was not the case with the viscous law, figure XI.9. The main purpose of the regularized approach is fulfilled: to remove the spurious mesh-dependency. However, there are no physical justifications for the choice of the specific regularization operator (122), nor for the strain regularization compared to other possible schemes enumerated in table XI.2.

2.3 ENHANCEMENT OF THE KINEMATICS: THE MICROMORPHIC CONTINUUM

One of the most general higher order continuum is the micromorphic one that adds to the displacement degrees of freedom $\vec{u}$ a full, non–symmetric, micro–deformation tensor $\underset{\sim}{\chi}$. The micro–deformation field is not necessarily compatible. If $\underset{\sim}{\chi}$ reduces to a pure rotation, the considered material is called a Cosserat medium. If one introduces the constraint that $\underset{\sim}{\chi}$ be equal to the gradient of the displacement field, the theory reduces to a second gradient model. The micromorphic theory therefore encompasses several other generalized models, which makes it an attractive framework to explore the regularization capabilities of enhanced continua. It is presented here within the small perturbation hypothesis. The reader is referred to Forest and Sievert (2003) for non–linear micromorphic models at finite strains.

2.3.1 Balance and constitutive equations

Several sets of generalized strain measures can be defined. The one used in Germain (1973) is retained here:

$$\underset{\sim}{\varepsilon} = \frac{1}{2}(\nabla\vec{u} + \nabla\vec{u}^T), \quad \underset{\sim}{\mathbf{e}} = \nabla\vec{u} - \underset{\sim}{\chi}, \quad \underset{\approx}{\boldsymbol{K}} = \nabla\,\underset{\sim}{\chi} \tag{126}$$

i.e. the strain, relative deformation and micro–deformation gradient tensors. Three generalized stress tensors must therefore be introduced in the virtual power of internal and contact forces:

$$p^{(i)} = \underset{\sim}{\sigma} : \dot{\underset{\sim}{\varepsilon}} + \underset{\sim}{\mathbf{s}} : \dot{\underset{\sim}{\mathbf{e}}} + \underset{\approx}{\boldsymbol{S}} \vdots \dot{\underset{\approx}{\boldsymbol{K}}}, \quad p^{(c)} = \vec{t}.\dot{\vec{u}} + \underset{\sim}{\mathbf{M}} : \dot{\underset{\sim}{\chi}} \tag{127}$$

where the stress tensor $\underset{\sim}{\sigma}$ is symmetric. The balance of momentum and balance of moment of momentum equations read:

$$\nabla(\underset{\sim}{\sigma} + \underset{\sim}{\mathbf{s}}) = \vec{0}, \quad \nabla\underset{\approx}{\boldsymbol{S}} + \underset{\sim}{\mathbf{s}} = 0 \tag{128}$$

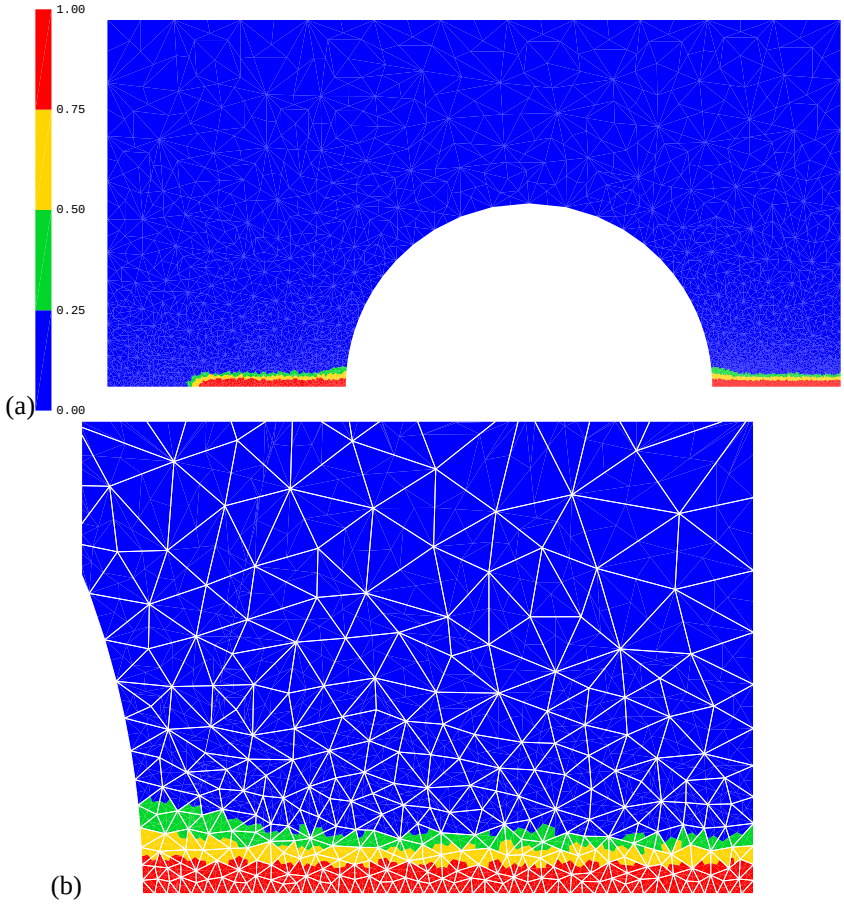

Figure XI.12: Damage field with the smoothed strain nonlocal model: (a) whole specimen, (b) close–up at the right side of the hole.

They are coupled thanks to the micro–stress tensor $\underset{\sim}{\mathbf{s}}$. Equilibrium at the boundary means:

$$\vec{t} = (\underset{\sim}{\sigma} + \underset{\sim}{\mathbf{s}}).\vec{n}, \quad \underset{\sim}{\mathbf{M}} = \underset{\approx}{\boldsymbol{S}}.\vec{n} \tag{129}$$

In the standard model, all strain tensors are decomposed independently into elastic and plastic contributions:

$$\underset{\sim}{\varepsilon} = \underset{\sim}{\varepsilon}^e + \underset{\sim}{\varepsilon}^p, \quad \underset{\sim}{\mathbf{e}} = \underset{\sim}{\mathbf{e}}^e + \underset{\sim}{\mathbf{e}}^p, \quad \underset{\approx}{\boldsymbol{K}} = \underset{\approx}{\boldsymbol{K}}^e + \underset{\approx}{\boldsymbol{K}}^p \tag{130}$$

The free energy is then a function of all elastic parts and additional internal variables: $\Psi(\underset{\sim}{\varepsilon}^e, \underset{\sim}{\mathbf{e}}^e, \underset{\approx}{\boldsymbol{K}}^e, q)$. The state laws read:

$$\underset{\sim}{\sigma} = \rho\frac{\partial\Psi}{\partial\,\underset{\sim}{\varepsilon}^e}, \quad \underset{\sim}{\mathbf{s}} = \rho\frac{\partial\Psi}{\partial\,\underset{\sim}{\mathbf{e}}^e}, \quad \underset{\approx}{\boldsymbol{S}} = \rho\frac{\partial\Psi}{\partial\underset{\approx}{\boldsymbol{K}}^e}, \quad R = \rho\frac{\partial\Psi}{\partial q} \tag{131}$$

The residual intrinsic dissipation follows:

$$D = \underset{\sim}{\sigma} : \dot{\underset{\sim}{\varepsilon}}^p + \underset{\sim}{\mathbf{s}} : \dot{\underset{\sim}{\mathbf{e}}}^p + \underset{\approx}{\boldsymbol{S}} \vdots \dot{\underset{\approx}{\boldsymbol{K}}}^p - R\dot{q} \tag{132}$$

The evolution equations can be derived from a viscoplastic potential $\Omega(\underset{\sim}{\sigma}, \underset{\sim}{\mathbf{s}}, \underset{\approx}{\boldsymbol{S}}, R)$:

$$\dot{\underset{\sim}{\varepsilon}}^p = \frac{\partial\Omega}{\partial\,\underset{\sim}{\sigma}}, \quad \dot{\underset{\sim}{\mathbf{e}}}^p = \frac{\partial\Omega}{\partial\,\underset{\sim}{\mathbf{s}}}, \quad \dot{\underset{\approx}{\boldsymbol{K}}}^p = \frac{\partial\Omega}{\partial\,\underset{\approx}{\boldsymbol{S}}}, \quad \dot{q} = -\frac{\partial\Omega}{\partial R} \tag{133}$$

The choice of a convex potential then ensures the positivity of intrinsic dissipation.

The viscoplastic potential can involve a single yield function containing a combination of all stress tensors, or, in contrast, be the sum of several mechanisms involving yield functions in which the individual stress tensors intervene separately. These two possibilities will be explored in the next subsection. Examples of single and multi–mechanism plasticity models for micromorphic media are provided in Chambon et al. (2001).

The main equations are summarized in table XI.3 in both intrinsic and index forms to avoid any ambiguity. The example of linear isotropic elastic relations is also provided, following Mindlin (1964). The general case of linear elasticity reads

$$\underset{\sim}{\sigma} = \underset{\approx}{\mathbf{c}} : \underset{\sim}{\varepsilon} + \underset{\approx}{\mathbf{g}} : \underset{\sim}{\mathbf{e}} \tag{134}$$

$$\underset{\sim}{\mathbf{s}} = \underset{\approx}{\mathbf{g}} : \underset{\sim}{\varepsilon} + \underset{\approx}{\mathbf{b}} : \underset{\sim}{\mathbf{e}} \tag{135}$$

$$\underset{\approx}{\boldsymbol{M}} = \underset{\approx\approx}{\mathbf{A}} \vdots \underset{\approx}{\boldsymbol{K}} \tag{136}$$

In the following, the coupling term will not be taken into account for simplicity. Simplified elasticity relations have been proposed in Shu and Fleck (1999) for the second grade medium:

$$\underset{\approx}{\boldsymbol{S}} = l_e^2\ \underset{\approx}{\mathbf{c}} : \underset{\approx}{\boldsymbol{K}}, \quad S_{ijk} = l_e^2 c_{ijpq} K_{pqk} \tag{137}$$

This relation can be used also for the micromorphic model and amounts to

$$A_1 = A_2 = A_3 = A_4 = A_5 = A_8 = l_e^2\lambda, \quad A_{10} = A_{11} = A_{13} = A_{14} = A_{15} = l_e^2\mu$$

This reduces the number of constants A_i (table XI.3) to a single internal length l_e.

Degrees of freedom

$$(\vec{u}, \underset{\sim}{\chi}) \qquad (u_i, \chi_{ij})$$

Strain measures

$$\underset{\sim}{\varepsilon} = {}^{\{}\nabla\vec{u}^{\}}, \quad \underset{\sim}{\mathbf{e}} = \nabla\vec{u} - \underset{\sim}{\chi} \qquad \varepsilon_{ij} = u_{(i,j)}, \quad e_{ij} = u_{i,j} - \chi_{ij}$$
$$\underset{\approx}{\boldsymbol{K}} = \nabla\,\underset{\sim}{\chi} \qquad K_{ijk} = \chi_{ij,k}$$

Balance equations

$$\nabla(\underset{\sim}{\sigma} + \underset{\sim}{\mathbf{s}}) + \vec{f} = 0, \quad \nabla\underset{\approx}{\boldsymbol{S}} + \underset{\sim}{\mathbf{s}} + \underset{\sim}{\mathbf{P}} = 0$$
$$(\sigma_{ij} + s_{ij})_{,j} + f_i = 0, \quad S_{ijk,k} + s_{ij} + P_{ij} = 0$$

Boundary conditions

$$\vec{t} = (\underset{\sim}{\sigma} + \underset{\sim}{\mathbf{s}}).\vec{n}, \quad \underset{\sim}{\mathbf{M}} = \underset{\approx}{\boldsymbol{S}}.\vec{n} \qquad t_i = (\sigma_{ij} + s_{ij})n_j, \quad M_{ij} = S_{ijk}n_k$$

Linear isotropic elasticity potential

$$\begin{aligned}
W &= \frac{1}{2}\lambda\varepsilon_{ii}\varepsilon_{jj} + \mu\varepsilon_{ij}\varepsilon_{ij} + \frac{1}{2}b_1 e_{ii}e_{jj} + \frac{1}{2}b_2 e_{ij}e_{ij} + \frac{1}{2}b_3 e_{ij}e_{ji} \\
&+ g_1\varepsilon_{ii}e_{jj} + g_2\varepsilon_{ij}(e_{ij} + e_{ji}) \\
&+ A_1 K_{iik}K_{kkj} + A_2 K_{iik}K_{jkj} + \frac{1}{2}A_3 K_{iik}K_{jkk} + \frac{1}{2}A_4 K_{ijj}K_{ikk} \\
&+ A_5 K_{ijj}K_{kik} + \frac{1}{2}A_8 K_{iji}K_{kjk} + \frac{1}{2}A_{10} K_{ijk}K_{ijk} \\
&+ A_{11} K_{ijk}K_{jki} + \frac{1}{2}A_{13} K_{ijk}K_{ikj} + \frac{1}{2}A_{14} K_{ijk}K_{jik} \\
&+ \frac{1}{2}A_{15} K_{ijk}K_{kji}
\end{aligned}$$

Linear isotropic elasticity relations

$$\sigma_{ij} = \lambda\varepsilon_{pp}\delta_{ij} + 2\mu\varepsilon_{ij} + g_1 e_{pp}\delta_{ij} + g_2(e_{ij} + e_{ji})$$
$$s_{ij} = g_1\varepsilon_{pp}\delta_{ij} + 2g_2\varepsilon_{ij} + b_1 e_{pp}\delta_{ij} + b_2 e_{ij} + b_3 e_{ji}$$

$$\begin{aligned}
S_{pqr} &= A_1(K_{rii}\delta_{pq} + K_{iip}\delta_{qr}) + A_2(K_{iiq}\delta_{pr} + K_{iri}\delta_{pq}) + A_3 K_{jjr}\delta_{pq} \\
&+ A_4 K_{pii}\delta_{qr} + A_5(K_{ipi}\delta_{qr} + K_{qii}\delta_{pr}) + A_8 K_{iqi}\delta_{pr} \\
&+ A_{10} K_{pqr} + A_{11}(K_{qrp} + K_{rpq}) + A_{13} K_{prq} \\
&+ A_{14} K_{qpr} + A_{15} K_{rqp}
\end{aligned}$$

Table XI.3: Micromorphic medium: balance equations and isotropic linear elasticity relations

2.3.2 Application to strain localization phenomena

Two extensions of the classical compressible plasticity framework with the elliptic potential presented in section 1.3.2 are proposed here.

Micromorphic plasticity with a single yield function

A yield criterion $g(\underset{\sim}{\sigma}, \underset{\sim}{\mathbf{s}}, \underset{\approx}{\boldsymbol{M}})$ is introduced that depends on the three stress tensors:

$$g(\underset{\sim}{\sigma}, \underset{\sim}{\mathbf{s}}, \underset{\approx}{\boldsymbol{M}}) = \sigma_\star - R(p) \tag{138}$$

$$\begin{aligned} \sigma_\star^2 &= \frac{3}{2} C\, \underset{\sim}{\sigma}^{dev} : \underset{\sim}{\sigma}^{dev} + F(\text{trace } \underset{\sim}{\sigma})^2 \\ &+ a_1\, \underset{\sim}{\mathbf{s}}^{dev} : \underset{\sim}{\mathbf{s}}^{dev} + a_2\, \underset{\sim}{\mathbf{s}}^{dev} : \underset{\sim}{\mathbf{s}}^{devT} + a_3(\text{trace } \underset{\sim}{\mathbf{s}})^2 + b \underset{\approx}{\boldsymbol{M}} \vdots \underset{\approx}{\boldsymbol{M}} \end{aligned} \tag{139}$$

The invariant $M_{ijk}M_{ijk}$ only is retained among the 5 possible ones for the sake of simplicity. The flow rules associated to the chosen yield function result from the generalized normality rule (133):

$$\dot{\underset{\sim}{\varepsilon}}^p = \dot{p} \frac{\partial g}{\partial\, \underset{\sim}{\sigma}}, \quad \dot{\underset{\sim}{\mathbf{e}}}^p = \dot{p} \frac{\partial g}{\partial\, \underset{\sim}{\mathbf{s}}}, \quad \dot{\underset{\approx}{\boldsymbol{K}}}^p = \dot{p} \frac{\partial g}{\partial \underset{\approx}{\boldsymbol{M}}} \tag{140}$$

The single plastic multiplier $\dot{p}$ is derived from the consistency condition when $g = 0$:

$$\dot{g} = \frac{\partial g}{\partial\, \underset{\sim}{\sigma}} : \dot{\underset{\sim}{\sigma}} + \frac{\partial g}{\partial\, \underset{\sim}{\mathbf{s}}} : \dot{\underset{\sim}{\mathbf{s}}} + \frac{\partial g}{\partial \underset{\approx}{\boldsymbol{M}}} \vdots \dot{\underset{\approx}{\boldsymbol{M}}} = 0 \tag{141}$$

$$\dot{p} = \frac{H_1}{H_2 + H_3 - H_4}, \quad \text{with} \quad H_1 = \frac{\partial g}{\partial\, \underset{\sim}{\sigma}} : \underset{\approx}{\mathbf{c}} : \dot{\underset{\sim}{\varepsilon}} + \frac{\partial g}{\partial\, \underset{\sim}{\mathbf{s}}} : \underset{\approx}{\mathbf{b}} : \dot{\underset{\sim}{\mathbf{e}}} + \frac{\partial g}{\partial \underset{\approx}{\boldsymbol{M}}} \vdots \underset{\approx\approx}{\mathbf{A}} \vdots \dot{\underset{\approx}{\boldsymbol{K}}} \tag{142}$$

$$H_2 = \frac{\partial g}{\partial\, \underset{\sim}{\sigma}} : \underset{\approx}{\mathbf{c}} : \frac{\partial g}{\partial\, \underset{\sim}{\sigma}} + \frac{\partial g}{\partial\, \underset{\sim}{\mathbf{s}}} : \underset{\approx}{\mathbf{b}} : \frac{\partial g}{\partial\, \underset{\sim}{\mathbf{s}}} + \frac{\partial g}{\partial \underset{\approx}{\boldsymbol{M}}} \vdots \underset{\approx\approx}{\mathbf{A}} \vdots \frac{\partial g}{\partial \underset{\approx}{\boldsymbol{M}}},$$

$$H_3 = \frac{dR}{dp}, \quad H_4 = \frac{\partial g}{\partial f}(1-f)\text{trace}\left(\frac{\partial g}{\partial\, \underset{\sim}{\sigma}}\right) \tag{143}$$

The contribution H_4 is due to the possible dependency of material parameters on porosity f, the evolution of which is still given by the classical formula: $\dot{f} = (1-f)\text{trace}\, \dot{\underset{\sim}{\varepsilon}}^p$.

Multi–criterion plasticity

According to this second class of elastoplastic models and in the spirit of multi–mechanism–based frameworks Mandel (1965); Cailletaud and Sai (1995), three equivalent stress measures are introduced, together with three distinct yield functions:

$$g_1(\underset{\sim}{\sigma}) = \sigma_\star - R(p), \quad g_2(\underset{\sim}{\mathbf{s}}) = s_\star - R_s(p_s), \quad g_3(\underset{\approx}{\boldsymbol{M}}) = M_\star - R_k(\kappa), \tag{144}$$

$$\sigma_\star^2 = \frac{3}{2} C\, \underset{\sim}{\sigma}^{dev} : \underset{\sim}{\sigma}^{dev} + F(\text{trace } \underset{\sim}{\sigma})^2 \tag{145}$$

$$s_\star^2 = \frac{3}{2} a_1 \underset{\sim}{\mathbf{s}}^{dev} : \underset{\sim}{\mathbf{s}}^{dev} + \frac{3}{2} a_2 \underset{\sim}{\mathbf{s}}^{dev} : \underset{\sim}{\mathbf{s}}^{devT} + a_3 (\text{trace } \underset{\sim}{\mathbf{s}})^2, \quad M_\star^2 = \underset{\approx}{\boldsymbol{M}} \vdots \underset{\approx}{\boldsymbol{M}} \tag{146}$$

The associative flow rules involve three plastic multipliers corresponding to each mechanism:

$$\dot{\underset{\sim}{\varepsilon}}^p = \dot{p} \frac{\partial g_1}{\partial \underset{\sim}{\sigma}}, \quad \dot{\underset{\sim}{\mathbf{e}}}^p = \dot{p}_s \frac{\partial g_2}{\partial \underset{\sim}{\mathbf{s}}}, \quad \dot{\underset{\approx}{\boldsymbol{K}}}^p = \dot{\kappa} \frac{\partial g_3}{\partial \underset{\approx}{\boldsymbol{M}}}, \quad \dot{p} = \frac{\frac{\partial g_1}{\partial \underset{\sim}{\sigma}} : \underset{\approx}{\mathbf{c}} : \dot{\underset{\sim}{\varepsilon}}}{\frac{\partial g_1}{\partial \underset{\sim}{\sigma}} : \underset{\approx}{\mathbf{c}} : \frac{\partial g_1}{\partial \underset{\sim}{\sigma}} + \frac{dR}{dp} - H_4} \tag{147}$$

$$\dot{p}_s = \frac{\frac{\partial g_2}{\partial \underset{\sim}{\mathbf{s}}} : \underset{\approx}{\mathbf{b}} : \dot{\underset{\sim}{\mathbf{e}}}}{\frac{\partial g_2}{\partial \underset{\sim}{\mathbf{s}}} : \underset{\approx}{\mathbf{b}} : \frac{\partial g_2}{\partial \underset{\sim}{\mathbf{s}}} + \frac{dR_s}{dp_s}}, \quad \dot{\kappa} = \frac{\frac{\partial g_3}{\partial \underset{\approx}{\boldsymbol{M}}} \vdots \underset{\approx}{\mathbf{A}} \vdots \dot{\underset{\approx}{\boldsymbol{K}}}}{\frac{\partial g_3}{\partial \underset{\approx}{\boldsymbol{M}}} \vdots \underset{\approx}{\mathbf{A}} \vdots \frac{\partial g_3}{\partial \underset{\approx}{\boldsymbol{M}}} + \frac{dR_k}{d\kappa}} \tag{148}$$

Coupling terms between the different mechanisms can be introduced in the hardening functions R, R_s et R_k. For simplicity, they are not considered here.

First application to strain localization phenomena

A micromorphic compressible elastoplastic material is considered, that admits a simple linear softening rule ($H < 0$):

$$R = R_0 + Hp$$

and an elliptic yield function. Plastic contributions $\underset{\sim}{\mathbf{e}}^p$ and $\underset{\approx}{\boldsymbol{K}}^p$ are set to zero in this first example. The classical plastic strain $\underset{\sim}{\varepsilon}^p$ only is non–vanishing. In this special case the previous two formulations of micromorphic plasticity coincide. It amounts to taking $a_1 = a_2 = a_3 = b = 0$ in equation (139), or very high thresholds R_s and R_k in equation (144). The remaining relevant parameters are the additional elastic moduli. One takes here:

$$b_1 = \lambda, \quad b_2 = b_3 = \mu, \quad A_{1,\ldots,15} = A \tag{149}$$

The classical parameters $\nu = 0$ and $F = C/2$ are used to ensure that no lateral deformation takes place and that strain localization bands are horizontal according to the classical bifurcation analysis of section 1.3.2. The problem becomes actually one–dimensional (strip along direction 2 in the sequel). The localization problem can in fact now be solved analytically.

$$\sigma_\star = \sqrt{C+F}\,|\sigma_{22}|, \quad \dot{\varepsilon}_{22}^p = \dot{p}\,\sqrt{C+F}, \quad \dot{p} = \frac{2\mu\sqrt{C+F}\,\dot{\varepsilon}_{22}}{2\mu(C+F)+H} \tag{150}$$

For monotonous loading, one gets:

$$p = \frac{2\mu\sqrt{C+F}}{2\mu(C+F)+H}\left(\varepsilon_{22} - \frac{R_0}{2\mu\sqrt{C+F}}\right) \tag{151}$$

The balance equations for stresses must be taken into account:

$$\begin{aligned} &(\sigma_{22} + s_{22})_{,2} = 0, \quad M_{222,2} + s_{22} = 0 \\ &\sigma_{22} = 2\mu(\varepsilon_{22} - \varepsilon_{22}^p) = \frac{2\mu}{2\mu(C+F)+H}\left(H\varepsilon_{22} + R_0\sqrt{C+F}\right), \\ &s_{22} = 2\mu(\varepsilon_{22} - \chi_{22}) \quad M_{222} = A\chi_{22,2} \end{aligned} \tag{152}$$

A system of equations is obtained for the two unknowns $(\varepsilon_{22}, \chi_{22})$:

$$\left\{ \begin{array}{c} \bar{H}\varepsilon_{22,2} + 2\mu(\varepsilon_{22,2} - \chi_{22,2}) = 0 \\ A\chi_{22,22} + 2\mu(\varepsilon_{22} - \chi_{22}) = 0 \end{array} \right. \tag{153}$$

where $\bar{H} = 2\mu H/(2\mu(C+F)+H)$. The micro–deformation χ_{22} is then solution of equation

$$\chi_{22,222} - \frac{2\mu\bar{H}}{A(\bar{H}+2\mu)}\,\chi_{22,2} = 0 \tag{154}$$

It appears that, when H is negative, the solution is sinusoidal with the wave length:

$$1/\omega = 1/\sqrt{\frac{2\mu|\bar{H}|}{A(\bar{H}+2\mu)}} \tag{155}$$

The strain discontinuity of figure XI.13(a) is replaced by a strain localization zone of finite width. The localization zone is an arc of sinus curve for this simple model, whereas the material unloads elastically in the rest of the strip.

Second application to strain localization phenomena

The multi–criterion model is used here with the following hardening rules:

$$R = R_0 + Hp, \quad R_s = R_{0s} + H_s p_s, \quad R_\kappa = R_{0\kappa} + H_\kappa l_p^2 \kappa \tag{156}$$

The modulus H is taken negative as in the previous examples, whereas H_s and $H_\kappa l_p^2$ remain positive. In addition to the parameters (149), the following values will be used in the numerical examples to come:

$$b_3 = \mu, \quad A = 25\ \mathrm{MPa.mm}^2, \quad a_1 = C = 1, \quad a_2 = 0, \quad a_3 = F = 0.5$$
$$H_s = 2\ \mathrm{MPa}, \quad H_\kappa = 50\ \mathrm{MPa}, \quad l_p = 1\ \mathrm{mm}$$
$$R_0 = 1\ \mathrm{MPa}, \quad R_{0s} = 0.0001\ \mathrm{MPa}, \quad R_{0\kappa} = 0.0001\ \mathrm{MPa.mm}^2 \tag{157}$$

The profile of the localization zone can again be predicted analytically. The analysis is similar to the previous one, when the elasticity relations are taken into account:

$$\sigma_{22} = \frac{2\mu}{2\mu(C+F)+H}(H\varepsilon_{22} + R_0\sqrt{C+F}) \tag{158}$$

$$s_{22} = \frac{2\mu}{2\mu(a_1+a_3)+H_s}(H_s e_{22} + R_{s0}\sqrt{a_1+a_3}) \tag{159}$$

$$M_{222} = \frac{A}{A+H_\kappa l_p^2}(H_\kappa l_p^2 K_{222} + R_{0\kappa}) \tag{160}$$

The following constants are defined:

$$\bar{H} = \frac{2\mu H}{2\mu(C+F)+H}, \quad \bar{H}_s = \frac{2\mu H_s}{2\mu(a_1+a_3)+H_s}, \quad \bar{H}_\kappa = \frac{AH_\kappa}{A+H_\kappa l_p^2} \tag{161}$$

The equation governing χ_{22} then takes the same form as (154). The strain localization profile is again a sinus arc with a wave length related to

$$\omega = \sqrt{\frac{|\bar{H}|\bar{H}_s}{\bar{H}_\kappa l_p^2(\bar{H}+\bar{H}')}} \tag{162}$$

2.3.3 Finite element simulations with the micromorphic continuum

The implementation of the micromorphic model into a finite element program is illustrated here in the two–dimensional case (plane stress and plane strain). The vector of degrees of freedom attributed to each node is written:

$$[\text{d.o.f}] = [U_1\ U_2\ X_{11}\ X_{22}\ X_{12}\ X_{21}]^T \tag{163}$$

The associated generalized strain vector is:

$$\begin{aligned}[\text{grad}] = \quad & [\varepsilon_{11}\ \varepsilon_{22}\ \varepsilon_{33}\ \varepsilon_{12}\ e_{11}\ e_{22}\ e_{33}\ e_{12}\ e_{21} \\ & K_{111}\ K_{112}\ K_{121}\ K_{122}\ K_{211}\ K_{212}\ K_{221}\ K_{222}]^T \end{aligned} \tag{164}$$

The matrix $[B]$ linking the strain vector to the degrees of freedom reads as follows under plane strain conditions:

$$[\text{grad}] = [B]\ [\text{d.o.f}]\,, \quad [B] = \begin{bmatrix} \partial_{x_1} & 0 & 0 & 0 & 0 & 0 \\ 0 & \partial_{x_2} & 0 & 0 & 0 & 0 \\ 0 & 0 & 0 & 0 & 0 & 0 \\ \frac{1}{2}\partial_{x_2} & \frac{1}{2}\partial_{x_1} & 0 & 0 & 0 & 0 \\ \partial_{x_1} & 0 & -1 & 0 & 0 & 0 \\ 0 & \partial_{x_2} & 0 & -1 & 0 & 0 \\ 0 & 0 & 0 & 0 & 0 & 0 \\ \partial_{x_2} & 0 & 0 & 0 & -1 & 0 \\ 0 & \partial_{x_1} & 0 & 0 & 0 & -1 \\ 0 & 0 & \partial_{x_1} & 0 & 0 & 0 \\ 0 & 0 & \partial_{x_2} & 0 & 0 & 0 \\ 0 & 0 & 0 & 0 & \partial_{x_1} & 0 \\ 0 & 0 & 0 & 0 & \partial_{x_2} & 0 \\ 0 & 0 & 0 & \partial_{x_1} & 0 & 0 \\ 0 & 0 & 0 & \partial_{x_2} & 0 & 0 \end{bmatrix} \tag{165}$$

where $\partial_{x_i} = \partial\cdot/\partial x_i$. Plane strain conditions imply $\varepsilon_{33} = e_{33} = 0$. In the case of plane stress conditions, ε_{33} and e_{33} are introduced as additional degrees of freedom shared by each element. The associated reactions are σ_{33} and s_{33}. Plane stress conditions are enforced by prescribing vanishing reaction stresses, but other conditions can also be considered. The generalized stress vector reads:

$$\begin{aligned}[\text{flux}] = \quad & [\sigma_{11}\ \sigma_{22}\ \sigma_{33}\ \sigma_{12}\ s_{11}\ s_{22}\ s_{33}\ s_{12}\ s_{21} \\ & M_{111}\ M_{112}\ M_{121}\ M_{122}\ M_{211}\ M_{212}\ M_{221}\ M_{222}]^T \end{aligned} \tag{166}$$

The isotropic elasticity matrix linking the elastic part of the micro–deformation gradient and the third–rank stress tensor is written as:

$$\begin{bmatrix} M_{111} \\ M_{112} \\ M_{121} \\ M_{122} \\ M_{211} \\ M_{212} \\ M_{221} \\ M_{222} \end{bmatrix} = [A] \begin{bmatrix} K_{111} \\ K_{112} \\ K_{121} \\ K_{122} \\ K_{211} \\ K_{212} \\ K_{221} \\ K_{222} \end{bmatrix}$$

where $[A]$ equals

$$\begin{bmatrix} AA & 0 & 0 & A_{1,4,5} & 0 & A_{2,5,8} & A_{1,2,3} & 0 \\ 0 & A_{3,10,14} & A_{2,11,13} & 0 & A_{1,11,15} & 0 & 0 & A_{1,2,3} \\ 0 & A_{2,11,13} & A_{8,10,15} & 0 & A_{5,11,14} & 0 & 0 & A_{2,5,8} \\ A_{1,4,5} & 0 & 0 & A_{4,10,13} & 0 & A_{5,11,14} & A_{1,11,15} & 0 \\ 0 & A_{1,11,15} & A_{5,11,14} & 0 & A_{4,10,13} & 0 & 0 & A_{1,4,5} \\ A_{2,5,8} & 0 & 0 & A_{5,11,14} & 0 & A_{8,10,15} & A_{2,11,13} & 0 \\ A_{1,2,3} & 0 & 0 & A_{1,11,15} & 0 & A_{2,11,13} & A_{3,10,14} & 0 \\ 0 & A_{1,2,3} & A_{2,5,8} & 0 & A_{1,4,5} & 0 & 0 & AA \end{bmatrix}$$

with $AA = 2A_1 + 2A_2 + A_3 + A_4 + 2A_5 + A_8 + A_{10} + 2A_{11} + A_{13} + A_{14} + A_{15}$. The notation $A_{i,j,k} = A_i + A_j + A_k$ is used.

The variational formulation of the micromorphic boundary value problem is a straightforward extension of the classical one:

$$\int_\Omega (\underset{\sim}{\varrho} : \dot{\underset{\sim}{\varepsilon}} + \underset{\approx}{\mathbf{s}} : \dot{\underset{\approx}{\mathbf{e}}} + \underset{\approx}{\boldsymbol{S}} \vdots \dot{\underset{\approx}{\boldsymbol{K}}})\, dV = \int_{\partial\Omega} (\vec{t}.\dot{\vec{u}} + \underset{\sim}{\mathbf{M}} : \dot{\underset{\sim}{\chi}})\, dS \tag{167}$$

with the boundary conditions $\vec{t} = (\underset{\sim}{\varrho} + \underset{\approx}{\mathbf{s}}).\vec{n}$, $\underset{\sim}{\mathbf{M}} = \underset{\approx}{\boldsymbol{S}}.\vec{n}$. The finite element formulation follows from the same discretization of the variational problem as in the classical case (Besson et al., 2001a).

The analytical solutions for the strain localization profiles derived in the previous sections are appropriate tests for the implementation of the model. The strip is meshed by a row of elements. Figure XI.14(a) shows that the numerical profile coincides with the predicted one according to equation (162). The mesh objectivity of the results can be tested also. In the classical case, mesh refinement leads to a strain localization band of smaller and smaller width, as shown on figure XI.13(a). In contrast, the localization band converges toward the predicted sinus arc for a sufficiently fine mesh (figure XI.13(b)).

The plasticity model based on a single yield function can be used now using the finite element method, for different values of parameter b allowing for non–vanishing plastic contribution K^p_{222}. The other parameters are set to the already given numerical values. In particular, $A_i = 1\ \mathrm{MPa.m}^2, \forall i$. The figure XI.14(b) gives the corresponding strain localization profiles. When b decreases, the band width tends toward one single finite element as in the classical case. No analytical solution is available for this model.

2.4 GRADIENT OF INTERNAL VARIABLES APPROACH

The introduction of the gradients of the internal variable is the last nonlocal approach that will be presented here. Once more, the new terms, based on spatial derivatives of some or all the internal variables, can be introduced in several ways, leading to various formulations. Therefore, to gain a unified framework, we rely again on the global variational formulation described in section 2.1. It means that we focus on generalized standard materials obeying the global constitutive laws (111)-(112).

2.4.1 Introduction of the gradient of internal variables

The homogenization assumption of scale separation has been pinpointed as the reason for the inadequacy of local constitutive behaviors in presence of localization. A minimal enrichment of the homogenization scheme based on internal variable gradients

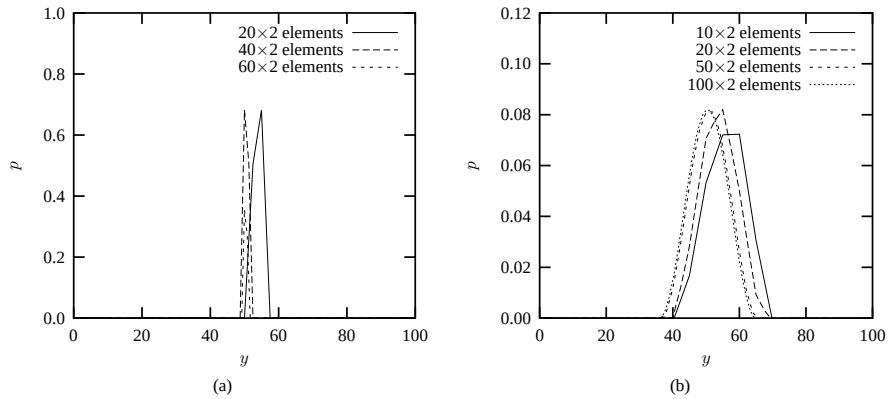

Figure XI.13: Finite element simulations of strain localization in a one–dimensional strip in tension using different mesh sizes: (a) classical plasticity model, (b) micromorphic plasticity model (the coordinate y describes the length of the strip).

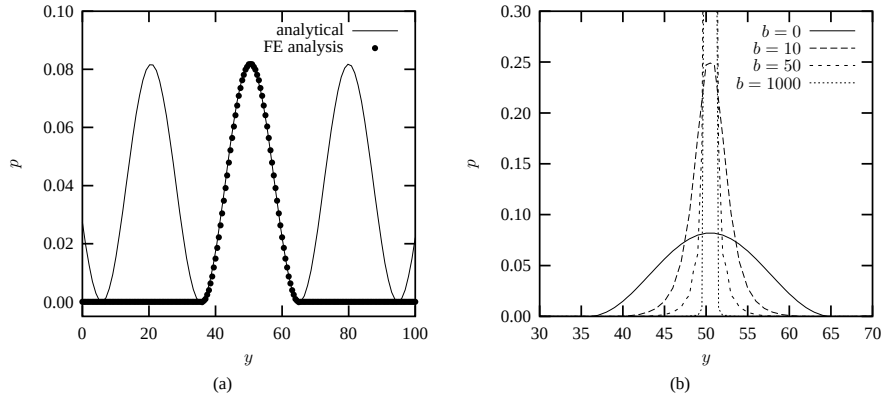

Figure XI.14: Simulation of strain localization in a strip made of a micromorphic elastoplastic material: (a) analytical and numerical solution for a multi–criterion model, (b) numerical results with a single–criterion micromorphic model for different values of material parameter b that intervenes in the yield function (139).

then relies on the involvement of the first order spatial gradient of the field of internal variables. At the scale of the material point, it results formally in a free energy and a dissipation potential that depend on an additional set of internal variables $b(\vec{x})$:

$$\Phi\left(\underset{\sim}{\varepsilon}(\vec{x}), a(\vec{x}), b(\vec{x})\right) \quad \text{and} \quad \Psi\left(\dot{a}(\vec{x}), \dot{b}(\vec{x})\right) \tag{168}$$

where $b(\vec{x})$ is the gradient of the field a:

$$b(\vec{x}) = \nabla a(\vec{x}) \tag{169}$$

It is interesting to note that a straightforward application of the local constitutive behavior (101)-(104) is generally not possible, as observed in Andrieux et al. (1996). Indeed, the evolution equations (103)-(104) would express the rates of the internal variables as functions of the material state and of the strain increment:

$$\begin{aligned} \dot{a}(x) &= G_a\left(\underset{\sim}{\varepsilon}(\vec{x}), a(\vec{x}), b(\vec{x}), \dot{\underset{\sim}{\varepsilon}}(\vec{x})\right) \\ \dot{b}(x) &= G_b\left(\underset{\sim}{\varepsilon}(\vec{x}), a(\vec{x}), b(\vec{x}), \dot{\underset{\sim}{\varepsilon}}(\vec{x})\right) \end{aligned} \tag{170}$$

The functions G_a and G_b could be given a closed-form but this proves useless here. Actually, the crucial point is the fact that to preserve the nonlocal relation (169) during the evolution of the internal variables, we should have:

$$\dot{b}(\vec{x}) = \nabla \dot{a}(\vec{x}) \;\Rightarrow\; G_b\left(\underset{\sim}{\varepsilon}(\vec{x}), a(\vec{x}), b(\vec{x}), \dot{\underset{\sim}{\varepsilon}}(\vec{x})\right) = \nabla G_a\left(\underset{\sim}{\varepsilon}(\vec{x}), a(\vec{x}), b(\vec{x}), \dot{\underset{\sim}{\varepsilon}}(\vec{x})\right)$$

This requirement puts severe and complex restrictions on the material state coupled to the strain evolution. This is in contradiction with the framework of generalized standard materials where no such restriction appears. It results indirectly from the fact that one of the main assumptions of the framework is not fulfilled: the independence of the state variables. Here, a and b are not independent since one is the gradient of the other. This deficiency justifies why the material point is not the appropriate scale to introduce nonlocality.

On the contrary, we define the global potentials as:

$$F\left(\underset{\sim}{\varepsilon},\ a\right) \underset{\text{def.}}{=} \int_\Omega \Phi\left(\underset{\sim}{\varepsilon}(\vec{x}),\ a(\vec{x}),\ \nabla a(\vec{x})\right) dx \tag{171}$$

$$D\left(\dot{a}\right) \underset{\text{def.}}{=} \int_\Omega \Psi\left(\dot{a}(\vec{x}),\ \nabla \dot{a}(\vec{x})\right) dx \tag{172}$$

Then, the set of internal variables is reduced to the single field a, so that the question of Independence is answered. The global constitutive law as defined in (111)-(112) is fully applicable. It is recalled:

$$\underset{\sim}{\sigma} = \frac{\partial F}{\partial \underset{\sim}{\varepsilon}}\left(\underset{\sim}{\varepsilon}, a\right) \qquad A = -\frac{\partial F}{\partial a}\left(\underset{\sim}{\varepsilon}, a\right) \tag{173}$$

$$A \in \partial D\left(\dot{a}\right) \tag{174}$$

Because of the introduction of the gradients, the formulation of the constitutive law at the structural scale and at the material point scale are no more equivalent. In particular,

the latter is flawed. The great difference with usual local laws is the fact that the evolution equation is now variational:

$$-\frac{\partial F}{\partial a}\left(\underset{\sim}{\varepsilon}, a\right) \in \partial D\left(\dot{a}\right) \tag{175}$$

Its solutions do not always admit a point wise characterization in terms of a flow rule and a consistency condition, depending on the expression of D. This definitely proves the interest of the minimum principle (120) to perform a numerical solution of the problem. Besides, the existence of solutions to (175) is proved in the context of dissipation potentials D which are positive homogeneous of degree one (rate-independent materials) as soon as they verify a coercivity property, in addition to the standard convexity and lower semi-continuity conditions, see Lorentz (1999).

Thermodynamic questions related to this class of constitutive relations are addressed in Lorentz and Andrieux (1999), especially the fact that the Clausius – Duhem inequality is only ensured at the structural scale. To retrieve a local positive dissipation, some nonlocality residual (Edelen and Laws, 1971; Polizzotto and Borino, 1998) or an extra entropy flux (Maugin, 1990) have to be introduced. However, a local definition of the dissipation does not seem necessary as long as no thermal coupling is taken into account.

2.4.2 Relation with gradient models of the literature

The definition of the potentials at the material point scale Φ and Ψ can be based either on phenomenological intuitions or homogenization derivations. For instance, Andrieux et al. (1996) provided some guidelines to derive the potentials from those corresponding to the local constitutive behavior, denoted Φ_{loc} and Ψ_{loc}. Namely, the additional gradient terms are quadratic. Relying on part of their results, we simply define the Helmholtz free energy and the dissipation potential as:

$$\Phi\left(\underset{\sim}{\varepsilon}(\vec{x}),\ a(\vec{x}),\ b(\vec{x})\right) \quad = \quad \Phi_{loc}\left(\underset{\sim}{\varepsilon}(\vec{x}),\ a(\vec{x})\right) + \frac{1}{2} c\, b(\vec{x})^2 \tag{176}$$

$$\Psi\left(\dot{a}(\vec{x}), \dot{b}(\vec{x})\right) \quad = \quad \Psi_{loc}\left(\dot{a}(\vec{x})\right) \tag{177}$$

In that special case, the variational evolution equation (175) does admit a point wise interpretation because the dissipation potential does not depend on the gradient of the internal variable rate.

Consider the global driving force A defined by (173). This linear form reads for any virtual field δa:

$$\begin{gathered}
\langle A \mid \delta a \rangle = -\left\langle \tfrac{\partial F}{\partial a} \;\middle|\; \delta a \right\rangle = \int_\Omega A_a(\vec{x})\, \delta a(\vec{x}) + A_b(\vec{x})\, \nabla \delta a(\vec{x}) \\
\text{with} \quad \left\{ \begin{array}{c} A_a(\vec{x}) = -\dfrac{\partial \Phi}{\partial a}\left(\underset{\sim}{\varepsilon}(\vec{x}), a(\vec{x}), \nabla a(\vec{x})\right) = -\dfrac{\partial \Phi_{loc}}{\partial a}\left(\underset{\sim}{\varepsilon}(\vec{x}), a(\vec{x})\right) \\ A_b(\vec{x}) = -\dfrac{\partial \Phi}{\partial b}\left(\underset{\sim}{\varepsilon}(\vec{x}), a(\vec{x}), \nabla a(\vec{x})\right) = -c\, \nabla a(\vec{x}) \end{array} \right.
\end{gathered} \tag{178}$$

After integration by parts, it can be expressed as:

$$\langle A \mid \delta a \rangle = \int_\Omega \left(A_a(\vec{x}) + c\, \nabla^2 a(\vec{x})\right)\, \delta a(\vec{x}) \quad - \int_{\partial\Omega} c\, \nabla a(\vec{x}) \cdot \vec{n}(\vec{x})\, \delta a(\vec{x}) \tag{179}$$

where $\partial\Omega$ and $\vec{n}$ denote respectively the boundary of the domain Ω and its outer normal. Following Ekeland and Temam (1974), it appears that satisfaction of (175) results in a zero boundary term in (179) and in the enforcement of the local evolution equation where $A_a(\vec{x}) + c\,\nabla^2 a(\vec{x})$ plays the role of the local driving force:

$$\left(A_a(\vec{x}) + c\,\nabla^2 a(\vec{x})\right) \in \partial\Psi_{loc}\left(\dot{a}(\vec{x})\right) \qquad \forall\ \vec{x} \in \Omega \tag{180}$$

The only nonlocal term is the laplacien of the internal variable field in the local evolution equation (180): the nonlocal model proposed and studied in Mühlhaus and Aifantis (1991) can be recognized. In this way, the model is recast in a more general framework. We think that departing from the variational formulation (173)-(174) instead of the point wise equations may give rise to new perspectives. Thus, the interpretation of the variational formulation also provides boundary and interface conditions. Namely, the vanishing boundary term in (179) leads to:

$$\nabla a(\vec{x}) \cdot \vec{n}(\vec{x}) = 0 \qquad \forall\ \vec{x} \in \partial\Omega \tag{181}$$

Moreover, by splitting the domain Ω in two sub-domains, it appears that the discontinuity of $A_b(\vec{x}) \cdot \vec{\nu}(\vec{x})$ across any interface of normal $\vec{\nu}$ should also be zero, that is:

$$[\![c\,\nabla a(\vec{x})]\!].\vec{\nu}(\vec{x}) = 0 \tag{182}$$

Finally, by requiring that the global free energy be finite, the internal variable field a has to belong to the Sobolev space $H^1(\Omega)$, so that its discontinuity across any interface is zero:

$$[\![a(\vec{x})]\!] = 0 \tag{183}$$

It is worth noticing that the boundary and the interface conditions are set on the damage field and not on its rate. This is a difference with most authors, see for instance de Borst and Mühlhaus (1992). In the context of gradient plasticity, they assigned the boundary and the interface conditions on the plastic strain rate, instead of the plastic strain itself. Consequently, along the free boundary between the elastic and the plastic zones, they did not take into account the interface condition (182), whose temporal derivative is difficult to postulate *a priori*. As an equation was missing in their model, they ended up with several solutions when they tried to solve the problem of a bar submitted to gradient plasticity. Therefore, they had to choose arbitrarily one of these solutions (the steepest one).

3 CASE STUDIES

3.1 NUMERICAL APPLICATION OF GRADIENT MODELS TO DUCTILE PLASTICITY

To illustrate the localization control provided by gradient models, the numerical simulation of a ductile notched specimen submitted to tension is performed, see figure XI.15. The constitutive law is based on the Rousselier model (see chapter VIII 4.2), which belongs to the framework of generalized standard materials. It is extended with new gradient terms in the spirit of the previous part.

Actually, the Rousselier model has to be given a slightly different presentation than usual to fully benefit from the global framework, see Lorentz and Cano (2003). The state variables consists of the total deformation gradient $\underset{\sim}{\mathbf{F}}$, the plastic deformation $\underset{\sim}{\mathbf{F}}^p$(multiplicative split of the deformation gradient) and a hardening variable p. The

local free energy Φ_{loc} is split in two terms, the elastic energy Φ_{el} which depends only on an elastic strain measure $\underset{\sim}{\mathbf{e}}$ (function of the total and the plastic strain) and a stored energy Φ_{st}, function of the hardening variable:

$$\Phi_{loc}\left(\underset{\sim}{\mathbf{F}}, \underset{\sim}{\mathbf{F}}^p, p\right) = \Phi_{el}\left(\underset{\sim}{\mathbf{e}}(\underset{\sim}{\mathbf{F}}, \underset{\sim}{\mathbf{F}}^p)\right) + \Phi_{st}\left(p\right) \tag{184}$$

The local evolution equation is governed by the principle of maximal dissipation with respect to the following threshold[3]:

$$g\left(\underset{\sim}{\mathbf{s}}, p\,;\ f\right) = s_{eq} + \sigma_1\, D\, f \exp\left(\frac{tr\underset{\sim}{\mathbf{s}}}{3\,\sigma_1}\right) - R\left(p\right) - \sigma^y \tag{185}$$

where $\underset{\sim}{\mathbf{s}}$ is a stress measure close to Kirchhoff stress tensor, which includes the volumetric change on the contrary of Cauchy stress, and f is the porosity. The corresponding dissipation potential can be found in Lorentz (1999), but its closed-form expression is not of great interest here. The porosity is not given the full status of an internal variable since it could be expressed as a function of the total deformation gradient under the micro-mechanical assumption of an incompressible matrix (with f_0 the initial porosity):

$$\frac{1-f_0}{1-f} = \det \underset{\sim}{\mathbf{F}} \tag{186}$$

The definitions (184) to (186) totally define the local constitutive behavior as soon as the formulation of finite strain proposed by Lorentz and Cano (2002) is adopted. It allows to retrieve the properties of generalized standard materials for finite strain, namely the characterization of the discretized constitutive law as a minimum principle.

The introduction of gradient terms follows the scheme proposed previously. Actually, only the hardening variable gradient is introduced because it proves sufficient to regularize the localization phenomenon. In that case, the free energy is equal to:

$$\Phi\left(\underset{\sim}{\mathbf{F}}, \underset{\sim}{\mathbf{F}}^p, p, \nabla p\right) = \Phi_{loc}\left(\underset{\sim}{\mathbf{F}}, \underset{\sim}{\mathbf{F}}^p, p\right) + \frac{1}{2} c\, \nabla p^2 \tag{187}$$

The numerical results are presented in figure XI.16 in terms of the porosity distribution, with the material characteristics given in table XI.17. It appears that a localization band initiates in the core of the specimen, in relation with the triaxiality distribution, then it propagates toward the notch. The width of the band is independent of the mesh size, on the contrary of the results obtained with the local model. Moreover, it is also proved independent of the mesh topology and the finite element type since the use of quadratic triangles allows to retrieve the same results as with under-integrated quadrangles.

Actually, special triangles are used to avoid locking phenomenon related to the "plastic incompressibility". They are based on a three field formulation (displacement, volumetric change, pressure) which proves totally compatible with the gradient formulation, see Michel-Ponnelle et al. (2003). The fact that triangle meshes are available to compute ductile structures is a very interesting point since it allows:

- automatic mesh generation in the case of structures with complex geometries ;
- automatic adaptive remeshing, in relation with an error criterion, to better capture the creation of localization bands without having to use a fine mesh everywhere a priori.

[3]This expression differs for the expression presented in chapter VIII because the Kirchhoff stress is used instead of the Cauchy stress.

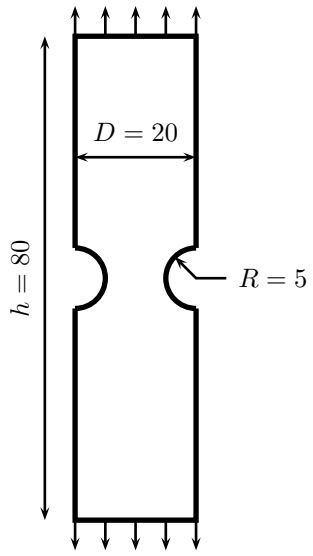

Figure XI.15: Notched specimen: geometry (in mm) and loading conditions.

In conclusion, these results definitely prove the potency of the gradient approach to perform real-life numerical simulations. However, the question of the agreement with experimental results in case of complex loading paths is still an open question which deserves future work.

3.2 DEFORMATION AND FRACTURE OF ALUMINUM FOAMS

Cellular materials are widely used for energy absorption applications Gibson and Ashby (1998). Depending on the wanted strength level, polymer or metal foams are good candidates for crash resistance applications in the automotive industry. The mechanical properties of aluminum foams obtained by injecting gas directly into the liquid metal is investigated in detail in Blazy (2003). It turns out that such foams are unable to deform in an homogeneous way. Instead, the short elastic regime is followed by the formation of intense strain localization bands that propagate through the whole specimen. Figure XI.18 shows that the bands are quasi–horizontal under compressive loading. The formation of the bands is associated with load drops on the overall load/displacement curves and their propagation is responsible for the observed plateau. The final stage is densification leading to a sharp increase of the load at the end of the localization process. The plastic behavior of metal foams is adequately modeled by an elliptic yield function as introduced in section 1.3.2 and proposed in Badiche et al. (2000); Deshpande and Fleck (2000). The horizontal orientation of the bands corresponds to the relation $F = C/2$ between the material parameters involved in the yield function (90). Multiaxial tests suggest that this is not necessarily true for the initial yield surface, but we will stick here to this simplification.

The formation of the first localization band is associated with an initial peak systematically observed on the overall curve of figure XI.19. The introduction of this first peak into the constitutive behavior by an appropriate dependency of the parameters C and F on porosity f triggers the formation of the first localization

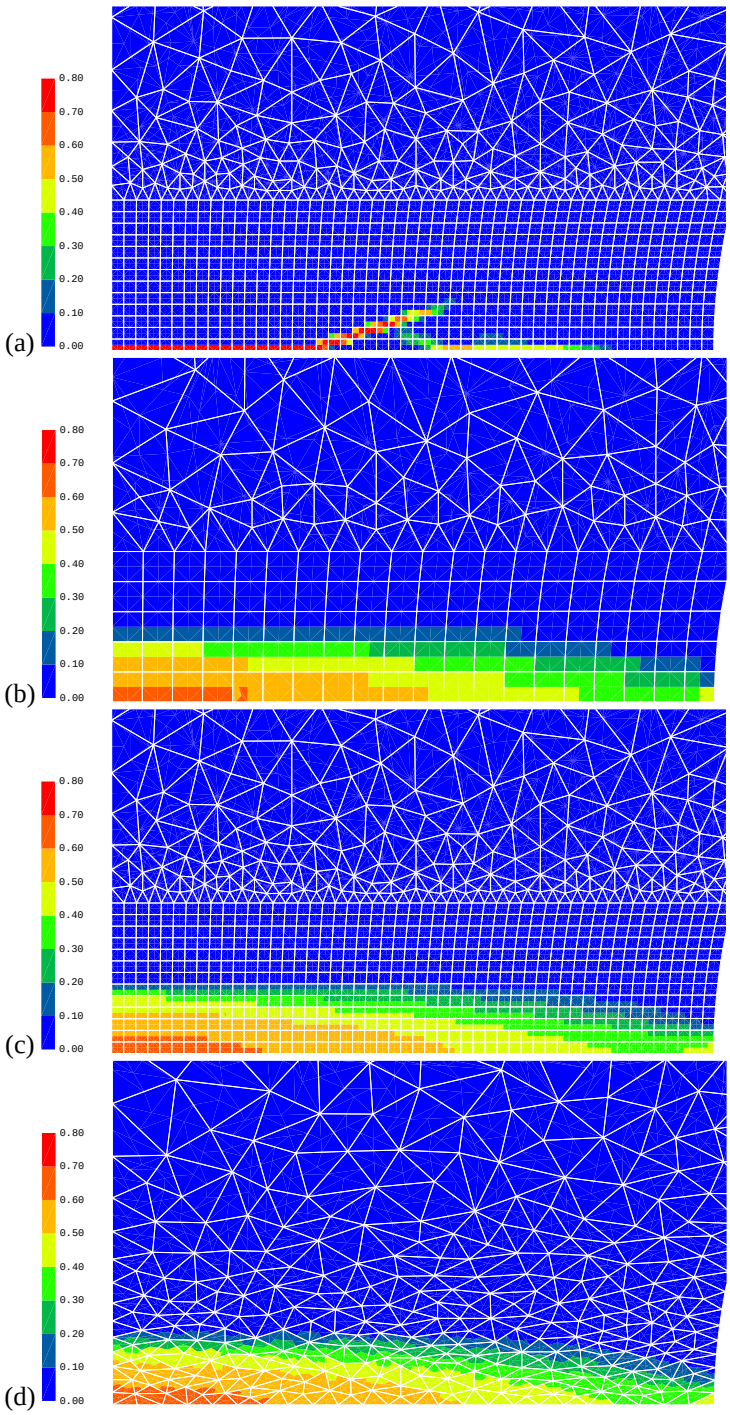

Figure XI.16: Porosity distribution (zoom) with the Rousselier model: (a) local law, (b,c,d) gradient laws.

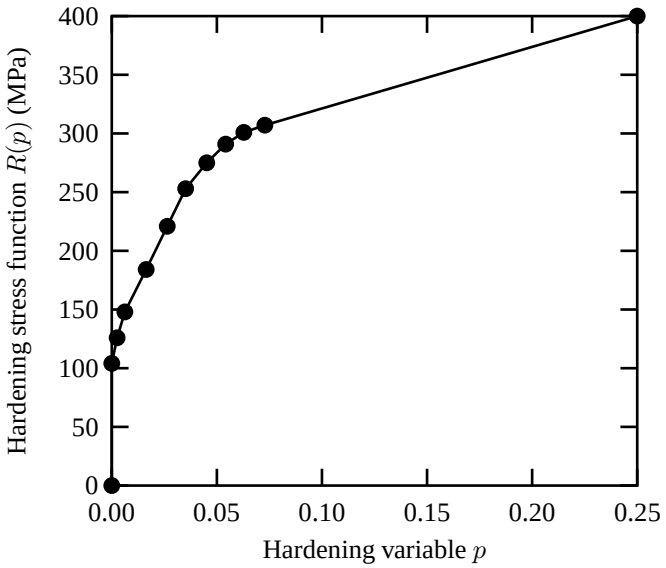

Figure XI.17: Material parameters for the Rousselier model

band. Densification then takes place inside the band, so that localization will occur again close to the band or at another location. This results in serrations on the simulated overall curve of figure XI.19. However, starting from a homogeneous initial porosity field and some initial material imperfections triggering localization is not sufficient to account for the slight apparent hardening observed on the experimental load/displacement curve. This is due to the tremendous heterogeneity of the initial porosity field induced by the foaming process, as shown on the view of figure XI.20(a) obtained by X–ray tomography. Efficient simulations of components made of aluminum foams require a continuum plasticity model that cannot account for the detailed distribution of large and small cells. Instead, it is proposed to replace the exact aluminum/air distribution by a smeared out porosity field. This is done by attributing to each material point of the image the mean density of a window of given size centered at this point. Such a smeared out porosity field is shown on figure XI.20(b) and used to initialize the finite element model of figure XI.20(c). The simulation of the compression of the sample then results in a complex distribution of strain localization bands that correctly mimic the experimental deformation process. The apparent hardening is then due to the successive crushing of zones of increasing local density inside the heterogeneous materials.

The simulation of such strain localization phenomena is necessary to predict the response of actual components made of metal foams to impacts for instance. The absence of localization in the simulation leads to significant overestimations of component strength.

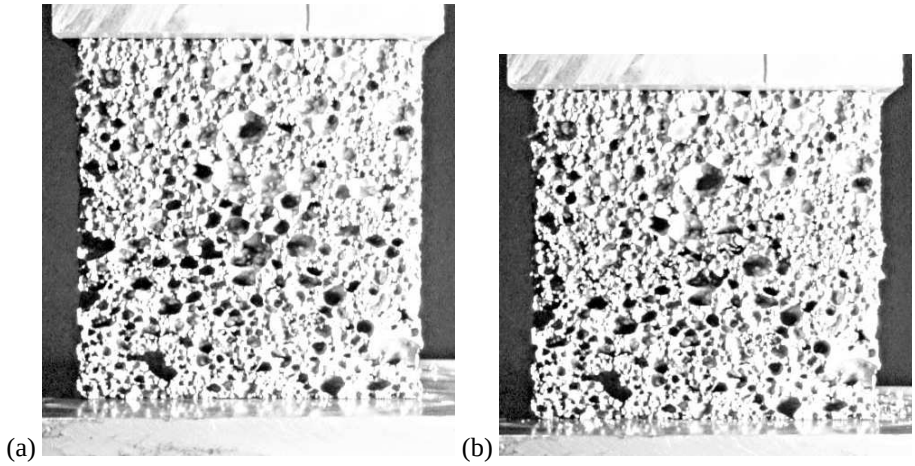

Figure XI.18: Strain localization in an aluminum foam under uniaxial compression: (a) initial state, (b) first strain localization band.

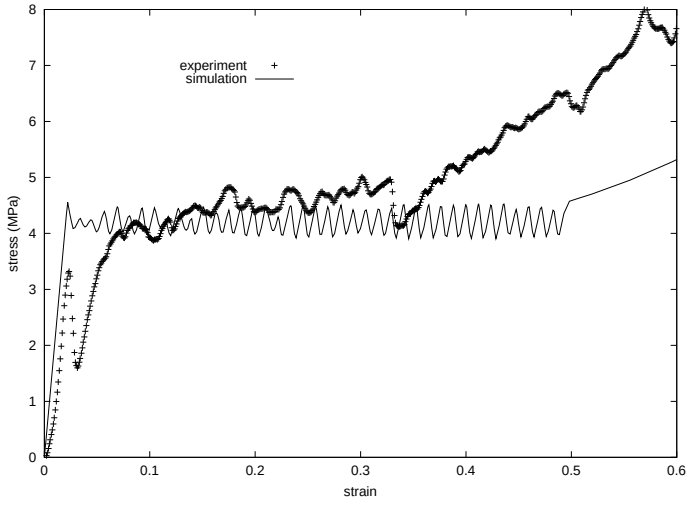

Figure XI.19: Experimental and simulated overall load/displacement curve for aluminum foam under compressive loading.

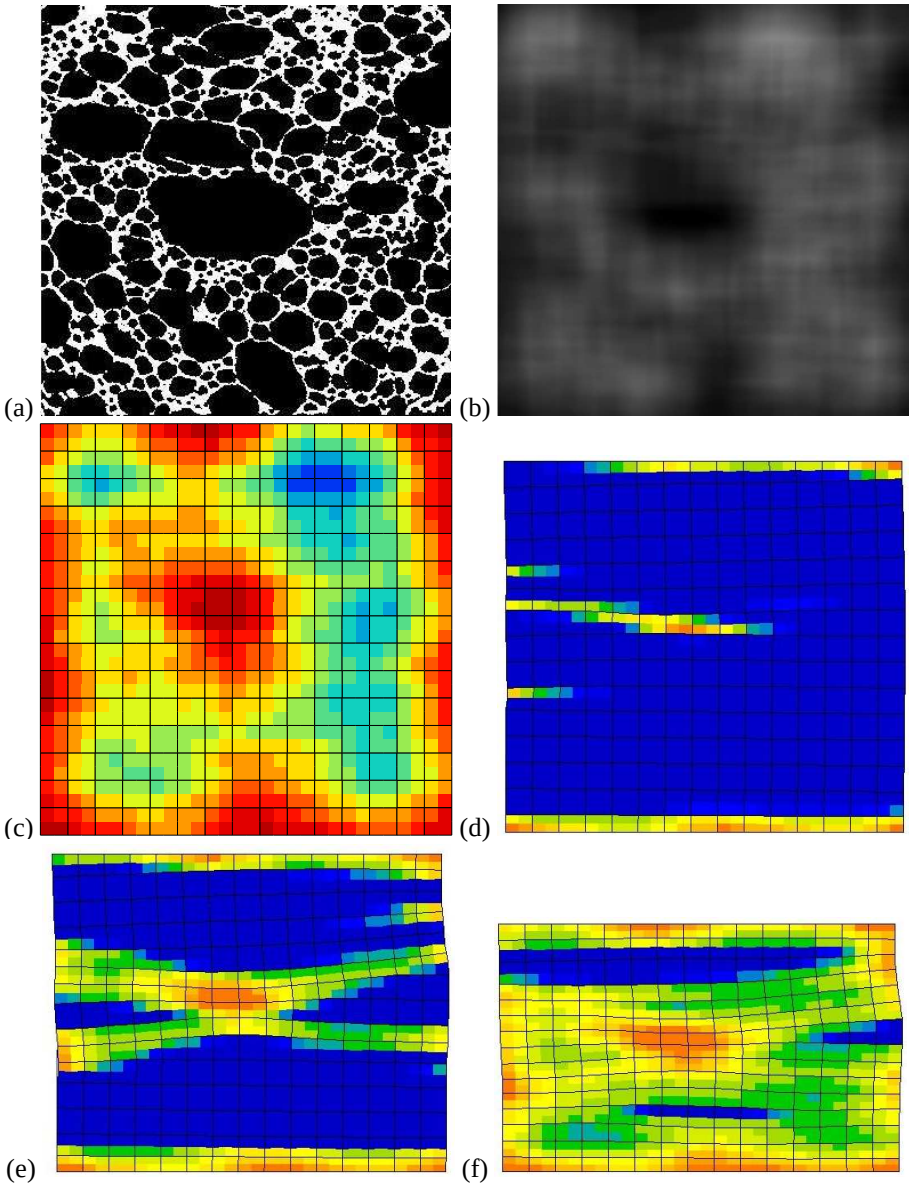

Figure XI.20: Simulation of strain localization during the compression of aluminum foam: (a) tomographical section of the initial state of the real sample, (b) smoothing of the porosity field using a moving averaging window (here a window of 60 pixels size), (c) initial porosity field attributed to the integration points of the mesh, (d,e,f) three stages of the strain localization process according to the simulation (the brown color indicates 60% axial strain; the image width is 2.5 cm).

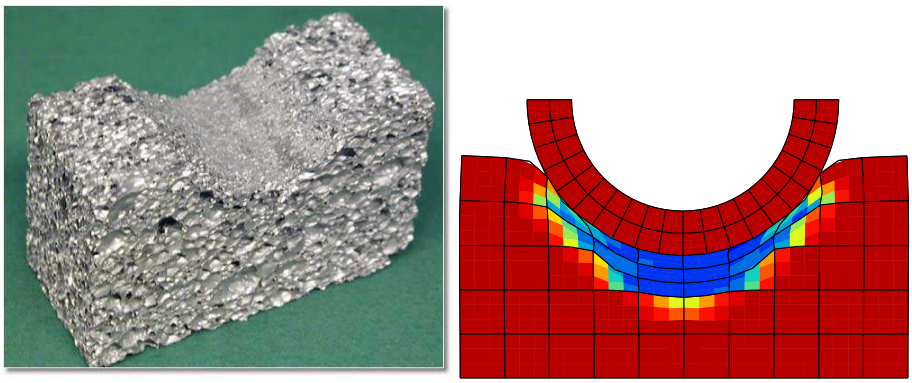

Figure XI.21: Simulation of cylindrical indentation of an aluminum foam: experimental and simulated results including the strain localization phenomena.

4 BIBLIOGRAPHY

Aifantis, E., 1987. The physics of plastic deformation. International Journal of Plasticity 3, 211–248.

Anand, L., Kim, K., Shawki, T., 1987. Onset of shear localization in viscoplastic solids. J. Mech. Phys. Solids 35, 407–429.

Andrieux, S., Joussemet, M., Lorentz, E., 1996. A class of constitutive relations with internal variable derivatives : derivation from homogenization. C. R. Acad. Sci., Série II b 323, 629–636.

Baaser, H., Tvergaard, V., 2003. A new algorithmic approach treating nonlocal effects at finite rate-independent deformation using the rousselier damage model. Comp. Meth. Appl. Mech. Engng 192, 107–124.

Badiche, X., Forest, S., Guibert, T., Bienvenu, Y., Bartout, J.-D., Ienny, P., Croset, M., Bernet, H., 2000. Mechanical properties and non-homogeneous deformation of open-cell nickel foams : application of the mechanics of cellular solids and of porous materials. Materials Science and Engineering A A289, 276–288.

Bardenhagen, S., Triantafyllidis, N., 1994. Derivation of higher order gradient continuum theories in 2,3-d non linear elasticity from periodic lattice models. Journal of the Mechanics and Physics of Solids 42, 111–139.

Bazant, Z., Pijaudier-Cabot, G., 1988. Non local continuum damage, localization instability and convergence. J. Appl. Mech. 55, 287–293.

Benallal, A., Billardon, R., Geymonat, G., 1989. Conditions de bifurcation à l'intérieur et aux frontières pour une classe de matériaux non-standards. C. R. Acad. Sci. Paris, Série II 308, 893–898.

Besson, J., Cailletaud, G., Chaboche, J.-L., Forest, S., 2001a. Mécanique non linéaire des matériaux. 445 p., Hermès, France.

Besson, J., Steglich, D., Brocks, W., 2001b. Modeling of crack growth in round bars and plane strain specimens. Int. J. Solids Structures 38 (46–47), 8259–8284.

Besson, J., Steglich, D., Brocks, W., 2003. Modeling of plane strain ductile rupture. Int. J. of Plasticity 19 (10), 1517–1541.

Bigoni, D., Hueckel, T., 1991. Uniqueness and localization: I Associative and nonassociative elastoplasticity. Int. J. Solids Structures 28, 197–214.

Billardon, R., Doghri, I., 1989. Prediction of macro-crack initiation by damage localization. C. R. Acad. Sci. Paris, Série II 308 (Série II), 347–352.

Blazy, J.-S., 2003. Comportement mécanique des mousses d'aluminium : caractérisations expérimentales sous sollicitations complexes et simulations numériques dans le cadre de l'élasto–plasticité compressible. Thèse de doctorat, Ecole des Mines de Paris.

Cailletaud, G., Sai, K., 1995. Study of plastic/viscoplastic models with various inelastic mechanisms. Int. J. of Plasticity 11 (8), 991–1005.

Chambon, R., Caillerie, D., Matsuchima, T., 2001. Plastic continuum with microstructure, local second gradient theories for geomaterials. Int. J. Solids Structures 38, 8503–8527.

Cherukuri, H., Shawki, T., 1995. An energy-based localization theory : I. basic framework. Int. J. Plasticity 11, 15–40.

Comi, C., 2001. A non-local model with tension and compression damage mechanisms. Eur. J. Mech., A/Solids 20, 1–22.

Comi, C., Perego, U., 2001. Numerical aspects of nonlocal damage analyses. Revue Européenne des Elements Finis 10, 227–242.

de Borst, R., 1991. Simulation of strain localization: a reappraisal of the Cosserat

continuum. Engng Computations 8, 317–332.
de Borst, R., 1993. A generalization of J_2-flow theory for polar continua. Computer Methods in Applied Mechanics and Engineering 103, 347–362.
de Borst, R., Mühlhaus, H., 1992. Gradient-dependent plasticity : formulation and algorithmic aspects. Int. J. Num. Meth. Engng 35, 521–539.
de Borst, R., Sluys, L., Mühlhaus, H., Pamin, J., 1993. Fundamental issues in finite element analyses of localization of deformation. Engineering Computations 10, 99–121.
Deshpande, V., Fleck, N., 2000. Isotropic constitutive models for metallic foams. Journal of Mechanics and Physics of solids 48, 1253–1283.
Desrues, J., Chambon, R., 1985. Bifurcation par localisation de la déformation : étude expérimentale et théorique de l'essai biaxial sur sable. In: Colloque international du CNRS : " déformation finie des agrégats : bases physiques et modélisations ".
Dobovsek, I., Moran, B., 1996. Material instabilities in rate dependent solids. Eur. J. Mech., A/Solids 15, 267–294.
Doghri, I., Billardon, R., 1995. Investigation of localization due to damage in elasto–plastic materials. Mechanics of Materials 19, 129–149.
Drugan, W., Willis, J., 1996. A micromechanics-based nonlocal constitutive equation and estimates of representative volume element size for elastic composites. Journal of the Mechanics and Physics of Solids 44, 497–524.
Duvaut, G., Lions, J.-L., 1976. Inequalities in Mechanics and Physics. Springer–Verlag.
Edelen, D., Laws, N., 1971. On the thermodynamics of systems with nonlocality. Arch. Rat. Mech. Anal 43, 24–35.
Ekeland, I., Temam, R., 1974. Analyse convexe et problèmes variationnels. Dunod Gauthier-Villars, Paris.
Eringen, A., 1972. Linear theory on nonlocal elasticity and dispersion of plane waves. Int. J. Engng. Sci 10, 425–435.
Eringen, A., 1976. Polar and non local fields theories, in Continuum Physics. Vol. IV. Academic Press.
Fleck, N., Hutchinson, J., 1993. A phenomenological theory for strain gradients effects in plasticity. J. Mech. Phys. Solids 41, 1825–1857.
Forest, S., Barbe, F., Cailletaud, G., 2000. Cosserat modelling of size effects in the mechanical behaviour of polycrystals and multiphase materials. International Journal of Solids and Structures 37, 7105–7126.
Forest, S., Sievert, R., 2003. Elastoviscoplastic constitutive frameworks for generalized continua. Acta Mechanica 160, 71–111.
Forest, S., van der Giessen, E., L. Kubin, Editors, 2001. Scale transitions from atomistics to continuum plasticity. J. Phys. IV, France, Vol. 11, Pr5, Les Editions de Physique.
Francfort, G., Marigo, J., 1993. Stable damage evolution in a brittle continuous medium. Eur. J. Mech., A/Solids 12, 149–189.
Fressengeas, C., Molinari, A., 1985. Inertia and thermal effects on the localisation of plastic flow. Acta Metall. 33, 387–396.
Gao, H., Huang, Y., Nix, W., Hutchinson, J., 1999. Mechanism-based strain gradient plasticity – i. theory. J. Mech. Phys. Solids 47, 1239–1263.
Germain, P., 1973. The method of virtual power in continuum mechanics. part 2 : Microstructure. SIAM J. Appl. Math. 25, 556–575.
Gibson, L., Ashby, M., 1998. Cellular solids. Cambridge University Press.
Godard, V., 2001. Modélisation mécanique non locale des matériaux fragiles :

délocalisation de la déformation. Tech. rep., Rapport de DEA, université Paris 6, France.

Gologanu, M., Leblond, J., Devaux, J., 1997. Continuum micromechanics. Vol. 377. Springer Verlag, CISM Courses and Lectures No. 377, Ch. Recent extensions of Gurson's model for porous ductile metals, pp. 61–130.

Halphen, B., Nguyen, Q., 1975. Sur les matériaux standards généralisés. Journal de Mécanique 14, 39–63.

Hill, R., 1958. A general theory of uniqueness and stability in elastic plastic solids. J. Mech. Phys. Solids 6, 236–249.

Hill, R., Hutchinson, J., 1975. Bifurcation phenomena in the plane tension test. J. Mech. Phys. Solids 23, 239–264.

Kröner, E., 1967. Mechanics of generalized continua, Proc. of the IUTAM-Symposium on the generalized Cosserat continuum and the continuum theory of dislocations with applications, Freudenstadt, Stuttgart. Springer Verlag.

Ladevèze, P., 2000. Constitutive relation error estimators for time-dependent non-linear fe analysis. Computer Methods in Applied Mechanics and Engineering 188, 775–788.

Leblond, J.-B., Perrin, G., Devaux, J., 1994. Bifurcation effects in ductile metals with nonlocal damage. Transactions of the ASME 61, 236–242.

Lemaitre, J., Chaboche, J.-L., 1994. Mechanics of Solid Materials. University Press, Cambridge, UK.

Lorentz, E., 1999. Lois de comportement à gradients de variables internes : construction par homogénéisation, formulation variationnelle et mise en oeuvre numérique. Thèse de doctorat, Université Paris 6.

Lorentz, E., Andrieux, S., 1999. A variational formulation for nonlocal damage models. Int. J. Plasticity 15, 119–138.

Lorentz, E., Andrieux, S., 2003. Analysis of nonlocal models through energetic formulations. Int. J. Solids Structures 40, 2905–2936.

Lorentz, E., Badel, P., 2003. A new path-following constraint for strain-softening finite element simulations. to appear in Int. J. Num. Meth. Engng 59.

Lorentz, E., Cano, V., 2002. A minimization principle for finite strain plasticity : Incremental objectivity and immediate implementation. Comm. Num. Meth. Engng 18, 851–859.

Lorentz, E., Cano, V., 2003. A nonlocal formulation applied to ductile damage. In: Benallal, A., Proenca, S., do Iguaçu, F. (Eds.), Proc. Symp. on recent developments in the modeling of rupture in solids, Brazil.

Mandel, J., 1962. Ondes plastiques dans un milieu indéfini à trois dimensions. J. de Mécanique 1, 3–30.

Mandel, J., 1965. Une généralisation de la théorie de la plasticité de W.T. Koiter. Int. J. Solids Structures 1, 273–295.

Mandel, J., 1966. Conditions de stabilité et postulat de drucker. In: Kravtchenko, J., Sirieys, P. (Eds.), Rhéologie et mécanique des sols. Springer Verlag.

Maugin, G., 1990. Internal variables and dissipative structures. J. Non–Equilib. Thermodyn. 15, 173–192.

Mear, M., Hutchinson, J., 1985. Influence of yield surface curvature on flow localization in dilatant plasticity. Mechanics of Materials 4, 395–407.

Michel-Ponnelle, S., Lorentz, E., Proix, J.-M., 2003. Calcul à fortes déformations plastiques : stratégie adaptative et éléments quasi-incompressibles de type tétraédrique. In: Potier-Ferry, M., Bonnet, M., Bignonnet, A. (Eds.), Proc. 6ème colloque national en calcul des structures de Giens.

Mindlin, R., 1964. Micro–structure in linear elasticity. Arch. Rat. Mech. Anal. 16, 51–78.

Mindlin, R., Eshel, N., 1968. On first strain gradient theories in linear elasticity. Int. J. Solids Structures 4, 109–124.

Moreau, J., 1970. Sur les lois de frottement, de plasticité et de viscosité. C. R. Acad. Sci., Série A 271, 608–611.

Mühlhaus, H., Aifantis, E., 1991. A variational principle for gradient plasticity. Int. J. Solids Structures 28, 845–857.

Needleman, A., 1988. Material rate dependence and mesh sensitivity in localization problems. Comp. Meth. Appl. Mech. Engng 67, 69–86.

Needleman, A., Ortiz, M., 1991. Effects of boundaries and interfaces on shear-band localization. Int. J. Solids Structures 28, 859–877.

Neilsen, M., Schreyer, H., 1993. Bifurcations in elastic–plastic materials. Int. J. Solids Structures 30, 521–544.

Nguyen, Q., 1993. Bifurcation and stability of dissipative systems. Springer Verlag, CISM Courses and Lectures No. 327, Ch. Bifurcation and stability of time-independent standard dissipative systems, pp. 45–94.

Nguyen, Q.-S., 2002. Stability and Nonlinear Solid Mechanics. Wiley.

Ottosen, N., Runesson, K., 1991a. Acceleration waves in elastoplasticity. Int. J. Solids Structures 28, 135–159.

Ottosen, N., Runesson, K., 1991b. Properties of discontinuous bifurcation solutions in elasto-plasticity. Int. J. Solids Structures 27, 401–421.

Peerlings, R., 1999. Enhanced damage modelling for fracture and fatigue. Phd thesis, Eindhoven University of Technology.

Peerlings, R., de Borst, R., Brekelmans, W., de Vree, J., 1996. Gradient-enhanced damage for quasi-brittle materials. Int. J. Num. Meth. Engng 39, 3391–3403.

Petryk, H., 1997. Instability of plastic deformation processes. In: Tatsumi, T. (Ed.), Proc. XIXth Congress of Theoretical and Applied Mechanics, Kyoto 1996. Elsevier.

Petryk, H., 2000. General conditions for uniqueness in materials with multiple mechanisms of inelastic deformation. J. Mech. Phys. Solids 48, 367–396.

Pijaudier-Cabot, G., Bazant, Z., 1987. Nonlocal damage theory. J. Engng Mech. 113, 1512–1533.

Pijaudier-Cabot, G., Huerta, A., 1991. Finite element analysis of bifurcation in non local softening. Comp. Meth. Appl. Mech. Engng 90, 905–919.

Polizzotto, C., Borino, G., 1998. A thermodynamics-based formulation of gradient-dependent plasticity. Eur. J. Mech., A/Solids 17, 741–761.

Raniecki, B., Bruhns, O., 1981. Bounds to bifurcation stresses in solids with non-associated plastic flow law at finite strain. J. Mech. Phys. Solids 29, 153–172.

Rice, J., 1976. The localization of deformation. In: Koiter, W. (Ed.), Theoretical and Applied Mechanics. North Publishing Company.

Rice, J., Rudnicki, J., 1980. A note on some features of the theory of localization of deformation. Int. J. Solids Structures 16, 597–605.

Rivalin, F., 1998. Développement d'aciers pour gazoducs à haute limite d'élasticité et ténacité élevée : Mécanique et mécanismes de la rupture ductile à grande vitesse. Ph.D. thesis, École des Mines de Paris.

Runesson, K., Mróz, Z., 1989. A note on non-associated flow rules. Int. J. of Plasticity 5, 639–658.

Shu, J., Fleck, N., 1999. Strain gradient crystal plasticity : size–dependent deformation of bicrystals. Journal of the Mechanics and Physics of Solids 47, 297–324.

Simo, J., 1988. Strain-softening and dissipation : a unification of approaches. In:

Bazant, Mazars (Eds.), Cracking and damage. Elsevier.
Stelmashenko, N., Walls, M., Brown, L., Milman, Y., 1993. Micro-indentations on W and Mo oriented single crystals : An stm study. Acta Metall. Mater. 41, 2855–2865.
Suo, Z., Ortiz, M., Needleman, A., 1992. Stability of solids with interfaces. J. Mech. Phys. Solids 40, 613–640.
Thomas, T., 1961. Plastic flow and fracture in solids. Academic Press.
Truesdell, C., Toupin, R., 1960. Handbuch der Physik, S. Flügge, editor, vol. 3. Springer verlag, Berlin, Ch. The classical field theories, pp. 226–793.
Tvergaard, V., Needleman, A., 1984. Analysis of the cup–cone fracture in a round tensile bar. Acta Mater. 32, 157–169.
Tvergaard, V., Needleman, A., 1995. Effects of nonlocal damage on a porous plastic solids. Int. J. Solids Structures 32, 1063–1077.

presses@dg.ensmp.fr

Local approach to fracture

By **Clotilde Berdin, Jacques Besson, Stéphane Bugat, Rodrigue Desmorat, Frédéric Feyel, Samuel Forest, Eric Lorentz, Eric Maire, Thomas Pardoen, André Pineau et Benoît Tanguy**
Under the supervision of **Jacques Besson**
ISBN : 2-911762-55-X, 430 pages, 16X24 cm
80 Euros
Prix spécial commande par Internet : 76 euros

Commander/ Order

Table des matières

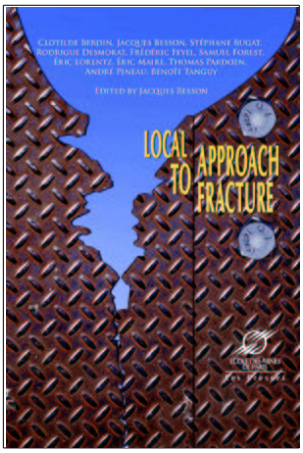

Résumé

Models allowing the prediction of the failure of structures by crack propagation were first introduced in the 50's using linear fracture mechanics whose principles were first proposed by Griffith (1920). This approach was extended to non linear cases (plasticity and viscoplasticity) in the 70's based on the work of Rice (J or C* integrals); it has been largely adopted by the industry. However this so called global approach cannot deal with all practical cases and cannot explain all experimental observations as, for instance, the warm pre-stress effect (WPS).

The local approach to fracture, which relies on a fine analysis of strains, stresses and damage of highly solicited regions (cracks, notches...) of structures is an alternative which allows to solve problems encountered while applying the global approach. It has been developped since the 80's in particular in France. Important research efforts are currently undertaken in this field in Europe (France, Germany), United States and Japan.

This book presents several aspects of the local approach to fracture: damage mechanisms, experimental techniques, damage evolution law and failure criteria, modelling of damage, numerical simulation.

This work is the result of a collective work carried out by the best french specialists (Ecole des Mines de Paris, Ecole Centrale Paris, ENS Cachan, Université de Louvain, INSA Lyon, ONERA, EDF).

Table des matières

Haut de page

Accueil